

A Novel 3-D Beam Domain Channel Model for Maritime Massive MIMO Communication Systems Using Uniform Circular Arrays

Yubei He¹, Cheng-Xiang Wang¹, *Fellow, IEEE*, Hengtai Chang¹, *Member, IEEE*, Rui Feng¹, *Member, IEEE*, Jian Sun¹, *Member, IEEE*, Wensheng Zhang¹, *Member, IEEE*, Yang Hao², *Fellow, IEEE*, and El-Hadi M. Aggoune³, *Life Senior Member, IEEE*

Abstract—In this paper, we first propose a 3-dimensional (3-D) non-stationary geometry-based stochastic model (GBSM) for maritime massive multiple-input multiple-output (MIMO) communication systems with the uniform circular array (UCA) configuration. To reduce the model complexity and improve the mathematical tractability, a novel beam domain channel model (BDCM) is then proposed based on the transformation of the corresponding GBSM from the array domain to the beam domain for maritime communications. In the proposed BDCM, the beamforming matrices suitable for UCA structures are constructed and their invertibility is demonstrated to ensure the practicability of the BDCM. Two methods are used to characterize the array non-stationarity in maritime massive MIMO channels. First, the evolution of clusters over the large UCA is modeled by the visibility regions (VRs) attached to individual multipath components (MPCs). Second, the sphere wavefront (SWF) effect is captured by dividing the UCAs into several sub-arrays. Based on the proposed GBSM and BDCM, some important channel statistical properties

are studied and compared, including channel power, power leakage, space-time-frequency correlation function (STF-CF), and root-mean-square (RMS) Doppler/beam spreads. Also, the importance of considering the array non-stationarity in maritime communication channels is revealed.

Index Terms—Maritime communications, beam domain channel model, geometry-based stochastic model, massive MIMO, uniform circular array.

I. INTRODUCTION

AS AN important part of the future sixth-generation (6G) space-air-ground-sea integrated communication networks, maritime communications are attracting the arising interests of researchers due to the rapid development of the marine economy [1], [2], [3]. Both traditional maritime industries and emerging tourism have put forward urgent demands for providing higher data rates [4], [5]. Massive MIMO, which can greatly improve the spectral/energy efficiency and user throughput, is a promising solution to enhance the performance of maritime wireless communication systems [6], [7], [8], [9]. Specially, considering the advantages over uniform linear arrays (ULAs) and uniform rectangular arrays (URAs), uniform circular arrays (UCAs) are usually employed in maritime wireless mesh networks to achieve energy bundling for longer distance transmission [10], [11]. In addition to providing a relatively compact structure, the geometric symmetries of UCAs can mitigate the mutual coupling effect and achieve uniform beam patterns around the azimuth angle. These features ensure that the beam shapes of UCAs do not change significantly in any direction [12], [13], [14], [15].

As the basic fundamental to constructing a maritime massive MIMO communication system using UCA, the characterization of maritime channels that considers the new channel characteristics brought by massive UCA should be conducted. For example, with the expansion of array size, the array stationarity assumption in conventional maritime MIMO channels is violated. The array non-stationarity including the sphere wavefront (SWF) effect and birth-death behaviors of clusters along the array axis should be considered. In addition, the usage of UCA will bring some unique channel characteristics. The effects of array configuration on channel characteristics need to be investigated. Some channel measurement campaigns using large-scale UCAs have

Manuscript received 9 July 2022; revised 13 December 2022; accepted 5 February 2023. Date of publication 15 February 2023; date of current version 18 April 2023. This work was supported by the National Key R&D Program of China under Grants 2018YFB1801101, the National Natural Science Foundation of China (NSFC) under Grants 61960206006 and 62071276, the Key Technologies R&D Program of Jiangsu (Prospective and Key Technologies for Industry) under Grants BE2022067 and BE2022067-1, the EU H2020 RISE TESTBED2 project under Grant 872172, the Natural Science Foundation of Shandong Province under Grant ZR2020MF002, and the University of Tabuk, Saudi Arabia under Grant 154-1444. The associate editor coordinating the review of this article and approving it for publication was J. M. Jornet. (*Corresponding authors: Cheng-Xiang Wang; Jian Sun.*)

Yubei He, Jian Sun, and Wensheng Zhang are with the Shandong Provincial Key Laboratory of Wireless Communication Technologies, School of Information Science and Engineering, Shandong University, Qingdao 266237, China (e-mail: heyubei@126.com; sunjian@sdu.edu.cn; zhangwsh@sdu.edu.cn).

Cheng-Xiang Wang is with the National Mobile Communications Research Laboratory, School of Information Science and Engineering, Southeast University, Nanjing 210096, China, and also with Purple Mountain Laboratories, Nanjing 211111, China (e-mail: chxwang@seu.edu.cn).

Hengtai Chang and Rui Feng are with Purple Mountain Laboratories, Nanjing 211111, China, and also with the National Mobile Communications Research Laboratory, School of Information Science and Engineering, Southeast University, Nanjing 210096, China (e-mail: changhengtai@pmlabs.com.cn; fengxiurui604@163.com).

Yang Hao is with the School of Electronic Engineering and Computer Science, Queen Mary University of London, E1 4NS London, U.K. (e-mail: y.hao@qmul.ac.uk).

El-Hadi M. Aggoune is with the Sensor Networks and Cellular Systems Research Center, University of Tabuk, Tabuk 47315, Saudi Arabia (e-mail: haggoune.sncs@ut.edu.sa).

Color versions of one or more figures in this article are available at <https://doi.org/10.1109/TCOMM.2023.3245662>.

Digital Object Identifier 10.1109/TCOMM.2023.3245662

0090-6778 © 2023 IEEE. Personal use is permitted, but republication/redistribution requires IEEE permission.

See <https://www.ieee.org/publications/rights/index.html> for more information.

been carried out. In [13] and [16], a virtual UCA with 720 antenna elements was exploited to analyze the spatial-temporal characteristics in indoor scenarios at sub-6 GHz and millimeter wave (mmWave) bands. The comparison of measured channel impulse responses (CIRs) over different array elements proved the existence of array non-stationarity. In [17] and [18], the channel characteristics of massive MIMO channels with 128-element virtual ULA and UCA in typical indoor and outdoor scenarios were compared. Based on the measurement results, the effects of antenna configuration on wireless channel were discussed. Besides, the visibility regions (VRs) of some scatterers were demonstrated to be not the whole array but only a part of the array. For maritime communication scenarios, massive MIMO communication systems with antenna panels have been used in some measurement campaigns [19], [20]. Nevertheless, the measurement results only focused on the system performance, and the channel measurement of maritime communications with massive UCAs is still lacking. Therefore, the channel characteristics of maritime massive MIMO communications, especially those with UCA configuration, need to be further studied.

The stochastic channel models for massive MIMO communications can be broadly divided into geometry-based stochastic models (GBSMs) and non-geometrical stochastic models (NGSMs). For GBSMs, the non-stationarity is generally modeled by the birth-death process or the VRs of clusters. For example, in [21], [22], and [23], the birth-death process was deployed to describe the evolution of scattering clusters on the array axis. While in [24] and [25], the concept of VR was introduced to determine the antennas that can see the clusters. These methods can capture the dynamic characteristics of clusters to some extent. However, these methods are all based on clusters and ignore the birth-death phenomenon of multipath components (MPCs) within clusters, which has been validated by the measurement results in [26]. As for the maritime communication scenarios, most existing maritime GBSMs mainly concentrate on the effect of the scattering environments and only support traditional MIMO communication channels [27], [28]. In [29], a twin-cluster maritime massive MIMO GBSM was proposed, which can characterize the marine environment properties and support the array/time non-stationarity. However, this model only considered the ULA configuration and there is still a lack of an appropriate maritime GBSM for massive MIMO communication channel with UCAs. Additionally, due to the considerable increase in the number of antennas, the number of radio frequency (RF) chains for massive MIMO systems will become dramatically large. This phenomenon will result in high hardware cost and transceiver complexity [30]. Correspondingly, the channel matrix of GBSM will become complicated.

Compared with GBSMs, the NGSMs, which mainly include the correlation-based stochastic models (CBSMs) and beam domain channel models (BDCMs), can usually provide simpler structures to facilitate signal processing research. For CBSMs, a simplified spatial correlation model of UCA was proposed in [31], and the closed-form expressions of

the spatial correlation matrices were derived. However, the model was built based on the simple distribution assumptions for the angles of arrival (AoAs) or the angles of departure (AoDs), and did not consider the non-stationarity in the array domain. Therefore, this kind of model is not suitable for characterizing maritime massive MIMO channels. From a practical point of view, the BDCMs were proposed and applied in [32], [33], [34], and [35]. Due to the limited number of nonzero channel elements, the BDCMs had obvious advantages in calculation complexity. The essence of BDCM is to transform the channel from the array domain into the beam domain with the help of beamforming matrices. This approach is inherently suitable for massive MIMO scenarios because the correlation of channel elements in BDCM decreases as the number of antennas increases. The multipath fading of each channel element can be approximately ignored when the number of antennas tends to infinity [36], [37]. Besides, the sparsity of maritime channel components makes BDCM and the maritime scenario a good fit. Based on the channel properties in the beam domain, the beam division multiple access (BDMA) transmission scheme was produced to obtain relatively low implementation complexity [36], [38]. However, most existing BDCMs focused only on ULA, which only supports 2-dimensional (2-D) space angular resolution. On the contrary, little attention has been paid to the discussion of UCA, which can inherently provide angular resolution in 3-dimensional (3-D) space. Furthermore, the spatial non-stationarity in BDCMs for massive MIMO systems with UCAs has not been fully investigated. The realistic BDCMs are the basis for measuring the performance of the emerging beam domain transmission technologies and their ability to be applied in maritime scenarios. Hence, it is necessary to build practical BDCMs for UCA maritime communication systems.

Motivated by the deficiencies in the current GBSMs and BDCMs for massive MIMO systems with UCAs in maritime communication scenarios, we propose a novel GBSM and a corresponding BDCM with the consideration of array non-stationarity to address the gaps mentioned above. In order to take full advantages of BDCMs, we will focus more on exploring the characteristics of maritime beam domain channels in the following sections. The novelties and main contributions of this paper are summarized as follows:

- A novel 3-D GBSM for maritime communication systems with the UCA configuration is proposed, which takes into account the array non-stationarity for massive MIMO communications. Then, by transforming the proposed GBSM from the array domain to the beam domain, a 3-D BDCM for maritime massive MIMO systems with UCAs is derived. The interconvertibility between the BDCM and GBSM is guaranteed by the invertibility of beamforming matrices.
- The VR method is introduced and the SWF effect is taken into account in the proposed GBSM and BDCM to reflect the array non-stationarity. The VR of each MPC in clusters is considered individually to mimic the evolution of MPCs over the UCAs.
- Key statistical properties of the proposed BDCM are derived and simulated, including channel power,

power leakage, space-time-frequency correlation function (STF-CF), and root-mean-square (RMS) Doppler/beam spreads. Both the theoretical and simulation results of the statistical properties verify the effect of array non-stationarity. Besides, their consistency verifies the correctness of both theoretical derivations and simulations. In addition, the STF-CF and Doppler spread of the corresponding GBSM are presented for comparisons.

The remainder of this paper is organized as follows. In Section II, a novel maritime massive MIMO GBSM considering near-field effect is proposed. In Section III, detailed derivations of the proposed 3-D BDCM for UCAs under both array stationary and array non-stationary conditions are given. Based on the proposed models, key statistical properties are derived in Section IV. In Section V, derivation and simulation results of those statistical properties are provided and compared. Finally, conclusions are drawn in Section VI.

II. A NOVEL GBSM FOR MASSIVE MIMO MARITIME COMMUNICATIONS WITH UCAs

Based on the ship-to-ship channel model in [29], we propose a novel maritime GBSM of the massive MIMO systems using UCAs. The simplified illustration of the GBSM is given in Fig. 1.

As shown in Fig. 1, we assume the UCAs are configured on the masts of ships as the transmitter (Tx) and receiver (Rx) to minimize the impact of hull blocking, and the ships move with velocities v^T and v^R , respectively. Considering the fluctuation characteristics of the actual sea surface and the motion of ships, the birth-death process of clusters in the time domain exists for maritime communication channels. The detailed derivation of the time non-stationarity can be found in [29]. To describe the movements of Tx and Rx in the 3-D space, the time-variant locations of the UCA centers at Tx and Rx in the global coordinate system (GCS) are denoted by the vectors $\mathbf{A}_c^T(t)$ and $\mathbf{A}_c^R(t)$. The effects of the velocities v^T and v^R are reflected in the changes of the UCA center locations. The angular positions of p -th ($p = 1, \dots, M_T$) Tx antenna element, i.e., A_p^T , and q -th ($q = 1, \dots, M_R$) Rx antenna element, i.e., A_q^R , are determined as $\phi_p^T = 2\pi(p-1)/M_T$ and $\phi_q^R = 2\pi(q-1)/M_R$. Without loss of generality, we assume that the origins of local coordinate systems (LCSs) are set at the centers of the UCAs and the antenna arrays are placed in the $x-y$ plane of LCSs. Then the positions of the antenna elements A_p^T and A_q^R in their LCSs can be expressed as $\mathbf{A}_p^T = [R_t \cos \phi_p^T, R_t \sin \phi_p^T, 0]$ and $\mathbf{A}_q^R = [R_r \cos \phi_q^R, R_r \sin \phi_q^R, 0]$, respectively, where R_t and R_r are the radii of the UCAs at Tx and Rx, respectively. Besides, the spacings between the adjacent antenna elements of Tx and Rx are denoted by d_t and d_r , respectively. Considering the maritime scattering environment generated from rough sea surface, other ships, duct effect, etc, the resulting multipath propagation between A_p^T and A_q^R can be abstracted as multi-bounce clusters propagation [39]. To make it clear, only the n -th ($n = 1, \dots, N$) scattering path is illustrated in the figure. For the n -th path, the first-bounce cluster C_n^A and the last-bounce cluster C_n^Z represent the scatterers near the Tx and

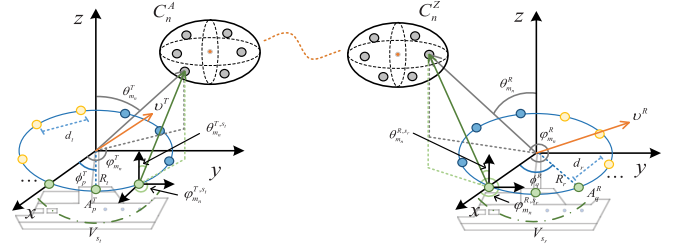


Fig. 1. Illustration of a 3-D massive MIMO maritime communication channel using UCAs.

Rx, respectively. The virtual delay $\tilde{\tau}_n$ is assumed to reflect the effect of the transmission link between C_n^A and C_n^Z . The virtual delay is drawn from exponential distribution, and the detailed derivation can be found in [40] and [41]. The azimuth AoD (AAoD) and zenith AoD (ZAoD) from the center of Tx to m -th ray in the n -th cluster are defined as $\varphi_{m,n}^T$ and $\theta_{m,n}^T$ in Fig. 1. The azimuth AoA (AAoA) and zenith AoA (ZAoA) from the center of Rx to m -th ray in the n -th cluster are obtained as $\varphi_{m,n}^R$ and $\theta_{m,n}^R$ according to the same definition principle. The locations of C_n^A and C_n^Z in GCS, i.e., $\mathbf{C}_n^A(t)$ and $\mathbf{C}_n^Z(t)$, can be determined by time-varying $\{\varphi_{m,n}^T, \theta_{m,n}^T\}$, $\{\varphi_{m,n}^R, \theta_{m,n}^R\}$, and randomly generated distances relative to the centers of the UCAs. The specific deduced process and corresponding stochastic distributions can be found in [29]. For the large size array, some clusters will be in the near-field range because of the increased Rayleigh distance, which leads to the SWF effect and cluster birth-death phenomenon on the array. To capture the angle drifting of the channel components over arrays caused by the SWF effect, the large UCAs are divided equally into $\{S_t, S_r\}$ sub-arrays of smaller size, which are distinguished by different colors in Fig. 1. Over different sub-arrays, the angular parameters of these clusters show variations, while that can be assumed to be constants over the antennas in the same sub-array considering the reduced Rayleigh distance of the sub-arrays. Then, the AAoD/AAoA and ZAoD/ZAoA from the antennas in s_t -th or s_r -th sub-array to m -th ray in the n -th cluster are defined as $\{\varphi_{m,n}^{T,s_t}, \varphi_{m,n}^{R,s_r}\}$ and $\{\theta_{m,n}^{T,s_t}, \theta_{m,n}^{R,s_r}\}$, respectively. The array evolution of clusters is modeled by VR method and will be discussed later. Besides, for the clusters in the far-field range, the angular parameters of MPCs on the whole array can be regarded as identical to satisfy the plane wavefront (PWF) assumption. The related parameters of the model are summarized in Table 1.

For the GBSM, the time-variant channel transfer function (CTF) between A_p^T and A_q^R can be modeled as

$$h_{p,q}(t, f) = \eta_{\text{LoS}}^{p,q} \cdot \sqrt{\frac{K}{K+1}} h_{p,q}^{\text{LoS}}(t, f) + \sum_{n=1}^{N(t)} \sum_{m_n=1}^{M_n} \eta_{m_n}^{p,q} \cdot \sqrt{\frac{\tilde{P}_{m_n}(t)}{K+1}} h_{p,q,m_n}^{\text{NLoS}}(t, f) \quad (1)$$

where $h_{p,q}^{\text{LoS}}(t, f)$ and $h_{p,q,m_n}^{\text{NLoS}}(t, f)$ are the line-of-sight (LoS) component and non-LoS (NLoS) component in the channel, respectively, K is the Ricean factor, $\tilde{P}_{m_n}(t)$ is the power of the m -th ray for the n -th path, $\{\eta_{\text{LoS}}^{p,q}, \eta_{m_n}^{p,q}\} \in \{0, 1\}$ are the visibility coefficients, and the values 1 and 0 indicate whether or not the channel component can be observed by the

TABLE I
DEFINITION OF THE MAIN CHANNEL PARAMETERS

Parameters	Definitions
N, M_n	The total number of paths between Tx and Rx and the total number of rays in the n -th cluster
C_n^A, C_n^Z	The first- and last-bounce clusters for the n -th scattering path, respectively
A_p^T, A_q^R	The p -th Tx antenna element and q -th Rx antenna element, respectively
ϕ_p^T, ϕ_q^R	The angular positions of the p -th Tx antenna element and q -th Rx antenna element
v^T, v^R	The velocities of Tx and Rx, respectively
S_t, S_r	The total numbers of the sub-arrays of Tx and Rx, respectively
V_{s_t}, V_{s_r}	The ranges of the s_t -th and s_r -th sub-arrays of Tx and Rx, respectively
$\{\varphi_{m_n}^T, \varphi_{m_n}^R\}, \{\theta_{m_n}^T, \theta_{m_n}^R\}$	AAoD/AAoA and ZAoD/ZAoA from the Tx/Rx array centers to m -th ray in the n -th cluster
$\{\varphi_{m_n}^{T,s_t}, \varphi_{m_n}^{R,s_r}\}, \{\theta_{m_n}^{T,s_t}, \theta_{m_n}^{R,s_r}\}$	AAoD/AAoA and ZAoD/ZAoA from s_t -th or s_r -th sub-array to m -th ray in the n -th cluster
R_t, R_r	The radii of the UCAs at Tx and Rx, respectively
d_t, d_r	The spacings of the Tx antenna elements and the Rx antenna elements, respectively

antenna pair A_p^T and A_q^R , respectively. In order to facilitate the representation, we think of the LoS path as 0-th cluster with only one ray, i.e., $n = 0$ and $M_0 = 1$. Then, the CTF can be written as

$$h_{p,q}(t, f) = \sum_{n=0}^{N(t)} \sum_{m_n=1}^{M_n} \eta_{m_n}^{p,q} \cdot \sqrt{P_{m_n}(t)} e^{j\Phi_{m_n}} \cdot e^{j2\pi(f_c - f)(\tau_{m_n}^c(t) + \tau_{m_n}^{p,q}(t))} \quad (2)$$

with

$$P_{m_n}(t) = \begin{cases} K \\ K+1 \end{cases}, \quad n = 0 \\ \frac{\tilde{P}_{m_n}(t)}{K+1}, \quad n = 1, \dots, N(t) \quad (3)$$

where f_c is the carrier frequency, P_{m_n} and Φ_{m_n} represent the general power coefficient and initial phase (uniformly distributed in $(0, 2\pi]$) of the m -th ray in the n -th cluster, $\tau_{m_n}^c$ is the transmission delay between the centers of UCAs at Tx and Rx through the m -th ray of the n -th path, and $\tau_{m_n}^{p,q}$ is the delay difference caused by the positions of p -th Tx antenna element and q -th Rx antenna element [12], [42]. The delay parameters can be calculated as

$$\tau_{m_n}^c(t) = \begin{cases} \|\mathbf{A}_c^R(t) - \mathbf{A}_c^T(t)\|/c, & n = 0 \\ (\|\mathbf{C}_{m_n}^A(t) - \mathbf{A}_c^T(t)\| + \|\mathbf{C}_{m_n}^Z(t) - \mathbf{A}_c^R(t)\|)/c + \tilde{\tau}_n, & n = 1, \dots, N(t) \end{cases} \quad (4)$$

$$\tau_{m_n}^{p,q}(t) \approx -(R_t \sin \theta_{m_n}^{T,s_t}(t) \cos(\varphi_{m_n}^{T,s_t}(t) - \phi_p^T) + R_r \sin \theta_{m_n}^{R,s_r}(t) \cos(\varphi_{m_n}^{R,s_r}(t) - \phi_q^R))/c \quad (5)$$

where c is the speed of light, s_t and s_r represent the parts of arrays to which the p -th Tx antenna element and q -th Rx antenna element belong. Because of the time-variant antenna and cluster locations, Doppler effect will appear in the channel.

The CTF matrix $\mathbf{H}(t, f) \in \mathbb{C}^{M_R \times M_T}$ of GBSM can be obtained as

$$\mathbf{H}(t, f) = \sum_{n=0}^{N(t)} \sum_{m_n=1}^{M_n} \sqrt{P_{m_n}(t)} e^{j\Phi_{m_n}} e^{j2\pi(f_c - f)\tau_{m_n}^c(t)} \cdot \mathbf{U}_{m_n}(t) \odot \mathbf{B}_{m_n} \quad (6)$$

where $\mathbf{U}_{m_n}(t) \in \mathbb{C}^{M_R \times M_T}$ is the response matrix for UCAs, \odot represents the Schur-Hadamard product, and \mathbf{B}_{m_n} is the visibility coefficient matrix indicating whether the m -th ray in the n -th cluster exists in the links between different Tx and Rx antenna elements. The response matrix $\mathbf{U}_{m_n}(t)$ can be determined as $\mathbf{U}_{m_n}(t) = [\mathbf{a}_{R,m_n}(t) \mathbf{a}_{T,m_n}^T(t)]^*$, where the response vectors [43] $\mathbf{a}_{R,m_n}(t)$ and $\mathbf{a}_{T,m_n}(t)$ are given in (7) and (8), respectively. The parameters $\mathbf{a}_R^{s_r}(\theta_{m_n}^{R,s_r}(t), \varphi_{m_n}^{R,s_r}(t))$ and $\mathbf{a}_T^{s_t}(\theta_{m_n}^{T,s_t}(t), \varphi_{m_n}^{T,s_t}(t))$ in (7) and (8), shown at the bottom of the page, are presented as (9) and (10), shown at the bottom of the page. In (9) and (10), λ is the carrier wavelength, $\{\phi_{s_r,s}^R, \phi_{s_t,s}^T\}$ and $\{\phi_{s_r,e}^R, \phi_{s_t,e}^T\}$ are the angular positions of the start and end elements of the s_t -th or s_r -th part in the Rx/Tx arrays, respectively, $[\cdot]^T$ denotes the transpose operation, and $[\cdot]^*$ denotes the conjugate operation. For the response vectors, the effect of frequency shift f on wavelength is approximately ignored since the frequency shift is much smaller than the carrier frequency.

According to the Rayleigh distance, i.e., $d_{r/t}^R = 2(2R_{r/t})^2/\lambda$, it can be judged whether the n -th cluster

$$\mathbf{a}_{R,m_n}(t) = \left[\mathbf{a}_R^1(\theta_{m_n}^{R,1}(t), \varphi_{m_n}^{R,1}(t)), \dots, \mathbf{a}_R^{s_r}(\theta_{m_n}^{R,s_r}(t), \varphi_{m_n}^{R,s_r}(t)), \dots, \mathbf{a}_R^{S_r}(\theta_{m_n}^{R,S_r}(t), \varphi_{m_n}^{R,S_r}(t)) \right]^T \quad (7)$$

$$\mathbf{a}_{T,m_n}(t) = \left[\mathbf{a}_T^1(\theta_{m_n}^{T,1}(t), \varphi_{m_n}^{T,1}(t)), \dots, \mathbf{a}_T^{s_t}(\theta_{m_n}^{T,s_t}(t), \varphi_{m_n}^{T,s_t}(t)), \dots, \mathbf{a}_T^{S_t}(\theta_{m_n}^{T,S_t}(t), \varphi_{m_n}^{T,S_t}(t)) \right]^T \quad (8)$$

$$\mathbf{a}_R^{s_r}(\theta_{m_n}^{R,s_r}(t), \varphi_{m_n}^{R,s_r}(t)) = \left[e^{j\frac{2\pi}{\lambda} R_r \sin \theta_{m_n}^{R,s_r}(t) \cos(\varphi_{m_n}^{R,s_r}(t) - \phi_{s_r,s}^R)}, \dots, e^{j\frac{2\pi}{\lambda} R_r \sin \theta_{m_n}^{R,s_r}(t) \cos(\varphi_{m_n}^{R,s_r}(t) - \phi_{s_r,e}^R)} \right] \quad (9)$$

$$\mathbf{a}_T^{s_t}(\theta_{m_n}^{T,s_t}(t), \varphi_{m_n}^{T,s_t}(t)) = \left[e^{j\frac{2\pi}{\lambda} R_t \sin \theta_{m_n}^{T,s_t}(t) \cos(\varphi_{m_n}^{T,s_t}(t) - \phi_{s_t,s}^T)}, \dots, e^{j\frac{2\pi}{\lambda} R_t \sin \theta_{m_n}^{T,s_t}(t) \cos(\varphi_{m_n}^{T,s_t}(t) - \phi_{s_t,e}^T)} \right] \quad (10)$$

experiences array non-stationary process, and from this, different forms of $\{\theta_{m_n}^{R,s_r}, \theta_{m_n}^{T,s_t}\}$, $\{\varphi_{m_n}^{R,s_r}, \varphi_{m_n}^{T,s_t}\}$, and \mathbf{B}_{m_n} are generated. Based on this, the CTF matrix $\mathbf{H}(t, f)$ can be rewritten as

$$\mathbf{H}(t, f) = \check{\mathbf{H}}(t, f) + \hat{\mathbf{H}}(t, f) \quad (11)$$

where $\check{\mathbf{H}}(t, f)$ and $\hat{\mathbf{H}}(t, f)$ represent the CTF matrices for the clusters that undergo and do not undergo the array non-stationary process, respectively. The BDCMs for $\check{\mathbf{H}}(t, f)$ and $\hat{\mathbf{H}}(t, f)$ will be discussed separately in the following.

III. A NOVEL BDCM FOR MASSIVE MIMO MARITIME COMMUNICATIONS WITH UCAS

The BDCM aims to describe the influence of MPCs on different beams and can be generated based on the corresponding GBSM utilizing the beamforming transform matrices. Here, we discuss the BDCMs of MPCs under different stationary conditions separately.

A. The 3-D BDCM for MPCs Under Array Stationary Condition

For the clusters under array stationary condition, the VRs should be the whole array and the PWF assumption holds. Therefore, the visibility coefficient matrix \mathbf{B}_{m_n} is a matrix of ones, and the AAoA/ZAoA and AAoD/ZAoD of each ray are similar for all the antenna elements in the Tx and Rx arrays, i.e., $\theta_{m_n}^{R,s_r}(t) = \theta_{m_n}^R(t)$, $\varphi_{m_n}^{R,s_r}(t) = \varphi_{m_n}^R(t)$, $s_r = 1, \dots, S_r$, and $\theta_{m_n}^{T,s_t}(t) = \theta_{m_n}^T(t)$, $\varphi_{m_n}^{T,s_t}(t) = \varphi_{m_n}^T(t)$, $s_t = 1, \dots, S_t$. Then, the CTF matrix $\hat{\mathbf{H}}(t, f)$ can be obtained as

$$\hat{\mathbf{H}}(t, f) = \sum_{n \in \mathbf{N}_1(t)} \sum_{m_n=1}^{M_n} \sqrt{P_{m_n}(t)} e^{j\Phi_{m_n}} e^{j2\pi(f_c - f)\tau_{m_n}^c(t)} \hat{\mathbf{U}}_{m_n}(t) \quad (12)$$

where $\mathbf{N}_1(t)$ is the set of the clusters under array stationary condition at time instant t , and the response vectors of $\hat{\mathbf{U}}_{m_n}(t) = [\hat{\mathbf{a}}_R(\theta_{m_n}^R(t), \varphi_{m_n}^R(t)) \hat{\mathbf{a}}_T^T(\theta_{m_n}^T(t), \varphi_{m_n}^T(t))]^*$, which can be simplified from (7) and (8), are provided in (13) and (14), shown at the bottom of the page.

Based on the beamforming operation of UCAs, the BDCM can be obtained from the proposed GBSM, i.e.,

$$\hat{\mathbf{H}}_B(t, f) = \tilde{\mathbf{U}}_R^T \hat{\mathbf{H}}(t, f) \tilde{\mathbf{U}}_T \quad (15)$$

where $\tilde{\mathbf{U}}_R$ and $\tilde{\mathbf{U}}_T$ are the beamforming matrices and can be expressed as

$$\tilde{\mathbf{U}}_R = \frac{1}{M_R} \left[\tilde{\mathbf{U}}_R^{(1)}, \tilde{\mathbf{U}}_R^{(2)}, \dots, \tilde{\mathbf{U}}_R^{(k_R)}, \dots, \tilde{\mathbf{U}}_R^{(K_R)} \right] \quad (16)$$

$$\tilde{\mathbf{U}}_T = \frac{1}{M_T} \left[\tilde{\mathbf{U}}_T^{(1)}, \tilde{\mathbf{U}}_T^{(2)}, \dots, \tilde{\mathbf{U}}_T^{(k_T)}, \dots, \tilde{\mathbf{U}}_T^{(K_T)} \right] \quad (17)$$

where $\tilde{\mathbf{U}}_R^{(k_R)}$ ($k_R = 1, \dots, K_R$) and $\tilde{\mathbf{U}}_T^{(k_T)}$ ($k_T = 1, \dots, K_T$) account for the azimuth beamforming matrices of the k_R -th and k_T -th zenith spatial beams, K_R and K_T are the total numbers of the zenith beams for Rx and Tx, respectively. The zenith beams are uniformly spaced samplings in $[0, \pi/2)$ with the spacing $\pi/(2K_R)$ and $\pi/(2K_T)$, i.e., $\tilde{\theta}_{k_R}^R = \frac{\pi(k_R-1)}{2K_R}$ and $\tilde{\theta}_{k_T}^T = \frac{\pi(k_T-1)}{2K_T}$. The azimuth beamforming matrix $\tilde{\mathbf{U}}_R^{(k_R)}$ and $\tilde{\mathbf{U}}_T^{(k_T)}$ can be defined as

$$\tilde{\mathbf{U}}_R^{(k_R)} = \left[\hat{\mathbf{a}}_R(\tilde{\theta}_{k_R}^R, \tilde{\varphi}_1^R), \dots, \hat{\mathbf{a}}_R(\tilde{\theta}_{k_R}^R, \tilde{\varphi}_{L_R}^R), \dots, \hat{\mathbf{a}}_R(\tilde{\theta}_{k_R}^R, \tilde{\varphi}_{L_R}^R) \right] \quad (18)$$

$$\tilde{\mathbf{U}}_T^{(k_T)} = \left[\hat{\mathbf{a}}_T(\tilde{\theta}_{k_T}^T, \tilde{\varphi}_1^T), \dots, \hat{\mathbf{a}}_T(\tilde{\theta}_{k_T}^T, \tilde{\varphi}_{L_T}^T), \dots, \hat{\mathbf{a}}_T(\tilde{\theta}_{k_T}^T, \tilde{\varphi}_{L_T}^T) \right] \quad (19)$$

where $\tilde{\varphi}_{l_R}^R = \frac{2\pi(l_R-1)}{L_R}$ ($l_R = 1, \dots, L_R$) and $\tilde{\varphi}_{l_T}^T = \frac{2\pi(l_T-1)}{L_T}$ ($l_T = 1, \dots, L_T$) are the azimuth beams, which are obtained as L_R and L_T uniformly spaced samplings of $[0, 2\pi)$. For the sake of clarity, the structure of beamforming matrix $\tilde{\mathbf{U}}_R$ is presented in Fig. 2, while $\tilde{\mathbf{U}}_T$ is similar to $\tilde{\mathbf{U}}_R$ in structure.

Combining (12) and (15)–(17), the channel element in the i' -th ($i' = 1, \dots, K_R L_R$) row and j' -th ($j' = 1, \dots, K_T L_T$) column of $\hat{\mathbf{H}}_B(t, f)$ can be obtained as (20), shown at the bottom of the page, where $J_0(\cdot)$ is the zero order Bessel function of the first kind, $\tilde{k} = \frac{2\pi}{\lambda}$ is the wave number, $k_R = \lceil \frac{i'}{L_R} \rceil$, $l_R = i' - (k_R - 1)L_R$, $k_T = \lceil \frac{j'}{L_T} \rceil$, and

$$\hat{\mathbf{a}}_R(\theta_{m_n}^R(t), \varphi_{m_n}^R(t)) = \left[e^{j\frac{2\pi}{\lambda} R_r \sin \theta_{m_n}^R(t) \cos(\varphi_{m_n}^R(t) - \phi_1^R)}, \dots, e^{j\frac{2\pi}{\lambda} R_r \sin \theta_{m_n}^R(t) \cos(\varphi_{m_n}^R(t) - \phi_{M_R}^R)} \right]^T \quad (13)$$

$$\hat{\mathbf{a}}_T(\theta_{m_n}^T(t), \varphi_{m_n}^T(t)) = \left[e^{j\frac{2\pi}{\lambda} R_t \sin \theta_{m_n}^T(t) \cos(\varphi_{m_n}^T(t) - \phi_1^T)}, \dots, e^{j\frac{2\pi}{\lambda} R_t \sin \theta_{m_n}^T(t) \cos(\varphi_{m_n}^T(t) - \phi_{M_T}^T)} \right]^T \quad (14)$$

$$\begin{aligned} \hat{h}_{i',j'}^B(t, f) &= [\tilde{\mathbf{U}}_R^T]_{i',:} \hat{\mathbf{H}}(t, f) [\tilde{\mathbf{U}}_T]_{:,j'} = \sum_{n \in \mathbf{N}_1(t)} \sum_{m_n=1}^{M_n} \sqrt{P_{m_n}(t)} e^{j\Phi_{m_n}} e^{j2\pi(f_c - f)\tau_{m_n}^c(t)} \\ &\times \frac{1}{M_R} \sum_{q=1}^{M_R} e^{j\frac{2\pi}{\lambda} R_r [\sin \tilde{\theta}_{k_R}^R \cos(\tilde{\varphi}_{l_R}^R - \phi_q^R) - \sin \theta_{m_n}^R(t) \cos(\varphi_{m_n}^R(t) - \phi_q^R)]} \\ &\times \frac{1}{M_T} \sum_{p=1}^{M_T} e^{j\frac{2\pi}{\lambda} R_t [\sin \tilde{\theta}_{k_T}^T \cos(\tilde{\varphi}_{l_T}^T - \phi_p^T) - \sin \theta_{m_n}^T(t) \cos(\varphi_{m_n}^T(t) - \phi_p^T)]} \\ &\approx \sum_{n \in \mathbf{N}_1(t)} \sum_{m_n=1}^{M_n} \sqrt{P_{m_n}(t)} e^{j\Phi_{m_n}} e^{j2\pi(f_c - f)\tau_{m_n}^c(t)} J_0(\tilde{k} \rho_{k_R, l_R}^{R, m_n}(t)) J_0(\tilde{k} \rho_{k_T, l_T}^{T, m_n}(t)) \end{aligned} \quad (20)$$

$l_T = j' - (k_T - 1)L_T$ are the beams corresponding to i' and j' , and $\{\rho_{k_R, l_R}^{R, m_n}(t), \rho_{k_T, l_T}^{T, m_n}(t)\}$ are defined as

$$\rho_{k_R, l_R}^{R, m_n}(t) = R_r \left[\left(\sin \tilde{\theta}_{k_R}^R \cos \tilde{\varphi}_{l_R}^R - \sin \theta_{m_n}^R(t) \cos \varphi_{m_n}^R(t) \right)^2 + \left(\sin \tilde{\theta}_{k_R}^R \sin \tilde{\varphi}_{l_R}^R - \sin \theta_{m_n}^R(t) \sin \varphi_{m_n}^R(t) \right)^2 \right]^{\frac{1}{2}} \quad (21)$$

$$\rho_{k_T, l_T}^{T, m_n}(t) = R_t \left[\left(\sin \tilde{\theta}_{k_T}^T \cos \tilde{\varphi}_{l_T}^T - \sin \theta_{m_n}^T(t) \cos \varphi_{m_n}^T(t) \right)^2 + \left(\sin \tilde{\theta}_{k_T}^T \sin \tilde{\varphi}_{l_T}^T - \sin \theta_{m_n}^T(t) \sin \varphi_{m_n}^T(t) \right)^2 \right]^{\frac{1}{2}}. \quad (22)$$

The detailed derivations of (20) are given in Appendix A.

In order to ensure the practicability and generality of the BDCM, the convertibility of BDCM to GBSM needs to be guaranteed, i.e., the beamforming matrices $\tilde{\mathbf{U}}_R$ and $\tilde{\mathbf{U}}_T$ should be invertible. Due to the special structures of the beamforming matrices, we only need to prove that there exists a left inverse for $\tilde{\mathbf{U}}_R^T$ and a right inverse for $\tilde{\mathbf{U}}_T$, i.e., $\tilde{\mathbf{U}}_R$ and $\tilde{\mathbf{U}}_T$ are row full rank matrices. In the proposed BDCM, we assume that the number of azimuth beams should be equal to the number of antennas, i.e., $L_R = M_R$ and $L_T = M_T$, to guarantee the invertibility of the beamforming matrices. Under this assumption, the azimuth beamforming matrices $\tilde{\mathbf{U}}_R^{(k_R)}$ and $\tilde{\mathbf{U}}_T^{(k_T)}$ are square matrices. In view of the variability of K_R and K_T , the right inverses of $\tilde{\mathbf{U}}_R$ and $\tilde{\mathbf{U}}_T$ can be considered to exist with probability one. The detailed proof can be found in Appendix B.

B. The 3-D BDCM for MPCs Under Array Non-Stationary Condition

For the clusters that can only be observed by some of the antenna elements of Tx and Rx, the entries in \mathbf{B}_{m_n} are determined by the VRs of MPCs [24], [37], which are introduced to describe the birth-death mechanism of MPCs along the array axis. It should be noticed that the entries in \mathbf{B}_{m_n} are 1 only if the m -th MPC in the n -th cluster can be observed by both A_p^T and A_q^R .

Different MPCs of a cluster have different birth-death behaviors on the arrays, thus it is necessary to generate VRs for each MPC separately. Besides, the VRs of the MPCs should be contained within the VRs of the corresponding clusters. Here, we first determine the VRs of clusters and then further discuss the evolution of MPCs. By considering the arrangement of antennas in UCAs, we assume the VRs are circular ranges, which can be determined by the center antennas and diameters. The center antennas of the VRs, denoted by $\{I_n^T, I_n^R\}$, follow uniform distributions [44], i.e., $I_n^T \sim \mathcal{U}[1, M_T]$ and $I_n^R \sim \mathcal{U}[1, M_R]$. The diameters of VRs, denoted by $\{r_n^T, r_n^R\}$, can be decided according to the exponential distribution, i.e., $r_n^T \sim \text{Exp}(\tilde{\lambda}^T)$ and $r_n^R \sim \text{Exp}(\tilde{\lambda}^R)$, where $\tilde{\lambda}^T$ and $\tilde{\lambda}^R$ are the rate parameters of exponential distributions for Tx and Rx arrays, respectively. Then, the VRs of MPCs ($V_{m_n}^T$ and $V_{m_n}^R$) are generated in the similar way. The center antennas

$\{I_{m_n}^T, I_{m_n}^R\}$ of $\{V_{m_n}^T, V_{m_n}^R\}$ follow uniform distribution and the diameters $\{r_{m_n}^T, r_{m_n}^R\}$ with respect to $\{r_n^T, r_n^R\}$ follow exponential distributions [24] which are controlled by the rate parameters $\tilde{\lambda}_M^T$ and $\tilde{\lambda}_M^R$. It should be noted that the positions of $\{I_{m_n}^T, I_{m_n}^R\}$ need to be restricted to the VRs of the corresponding clusters. Besides, the distribution of center antennas and VR diameters can be adjusted according to specific scenarios. A simplified example of the VR generation process is shown in Fig. 3. In the simulations of Fig. 3, the rate parameters are obtained from [24]. Without loss of generality, the distance between two adjacent antenna elements is assumed to be half a wavelength. Then the radii of Tx and Rx UCAs can be calculated as [30]

$$R_{r/t} = \frac{\lambda}{2\sqrt{2 - 2\cos\left(\frac{2\pi}{M_{R/T}}\right)}}. \quad (23)$$

As illustrated in Fig. 3, the VRs of different clusters are distributed in different areas of the array and there may be overlap between VRs such as cluster 2 and cluster 4. The circle with a dashed line represents the VR of cluster 4 and the VRs of two MPCs in cluster 4 are circled by dot dash lines. The antennas inside the circle of each MPC are considered to be able to observe the MPC and the corresponding entries of the antennas in \mathbf{B}_{m_n} are set as 1, while other entries are set as 0. It is important to highlight that though the VRs of some MPCs are beyond the VRs of their corresponding clusters, there is no need to consider the out-of-range antennas due to the limitation of the clusters' VRs on the MPCs' VRs.

Therefore, the CTF matrix $\check{\mathbf{H}}(t, f)$ needs to account for the effect of the visibility coefficient matrix, and can be written as

$$\check{\mathbf{H}}(t, f) = \sum_{n \in \mathbf{N}_2(t)} \sum_{m_n=1}^{M_n} \sqrt{P_{m_n}(t)} e^{j\Phi_{m_n}} e^{j2\pi(f_c - f)\tau_{m_n}^c(t)} \cdot \mathbf{U}_{m_n}(t) \odot \mathbf{B}_{m_n} \quad (24)$$

where $\mathbf{N}_2(t)$ is the set of the clusters under array non-stationary condition at the time instant t .

After a similar process, the BDCM for $\check{\mathbf{H}}(t, f)$ can be obtained as

$$\check{\mathbf{H}}_B(t, f) = \tilde{\mathbf{U}}_R^T \check{\mathbf{H}}(t, f) \tilde{\mathbf{U}}_T \quad (25)$$

where the channel element of $\check{\mathbf{H}}_B(t, f)$ can be expressed as (26), shown at the bottom of the next page, with

$$\begin{aligned} \check{J}_{m_n}^{k_R, l_R}(t) &= \sum_{s_r=1}^{S_r} \sum_{a=-\infty}^{\infty} f_{m_n}^{s_r}(a) e^{ja(\pi/2 - \xi_{k_R, l_R}^{s_r, m_n}(t))} \\ &\quad \times J_a(\tilde{k} \rho_{k_R, l_R}^{s_r, m_n}(t)) \\ \check{J}_{m_n}^{k_T, l_T}(t) &= \sum_{s_t=1}^{S_t} \sum_{b=-\infty}^{\infty} f_{m_n}^{s_t}(b) e^{jb(\pi/2 - \xi_{k_T, l_T}^{s_t, m_n}(t))} \\ &\quad \times J_b(\tilde{k} \rho_{k_T, l_T}^{s_t, m_n}(t)) \end{aligned} \quad (27)$$

where $V_{m_n}^{R, s_r} = V_{m_n}^R \cap V_{s_r}$ and $V_{m_n}^{T, s_t} = V_{m_n}^T \cap V_{s_t}$ represent the ranges of antennas that exist in both the VRs of the MPCs in \mathbf{N}_2 and the s_r -th or s_t -th partition of the Rx/Tx arrays, $J_{\tilde{n}}(x) = (1/\pi) \int_0^\pi \cos(\tilde{n}\alpha - x \sin \alpha) d\alpha$ is the \tilde{n} -th order Bessel function of the first kind, $f_{m_n}^{s_r}(a)$

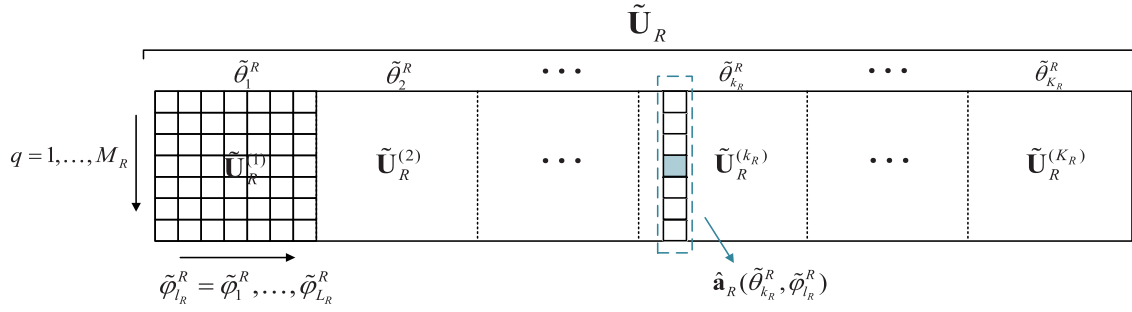


Fig. 2. The structure of the 3-D beamforming matrix for Rx.

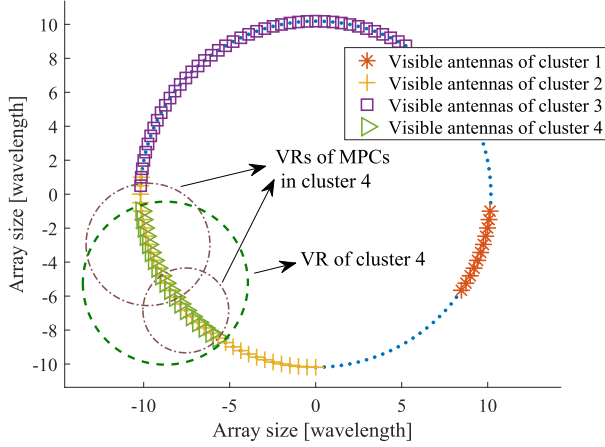


Fig. 3. A simplified diagram showing the VRs of clusters.

and $f_{m_n}^{st}(b)$ are the coefficients that can determine the influence of Bessel functions of different orders. The detailed derivation of $\{f_{m_n}^{sr}(a), f_{m_n}^{st}(b)\}$, $\{\xi_{k_R, l_R}^{sr, m_n}(t), \xi_{k_T, l_T}^{st, m_n}(t)\}$, and $\{\rho_{k_R, l_R}^{sr, m_n}(t), \rho_{k_T, l_T}^{st, m_n}(t)\}$ is also given in Appendix A. Since $f_{m_n}^{sr}(a)$ and $f_{m_n}^{st}(b)$ are complex weighted Dirichlet sinc functions [45] on the orders of Bessel functions, the zero order Bessel function is still the principal term. However, some low-order Bessel functions and the angular drifting on different partitions of arrays also introduce a non-negligible effect, which will result in power leakage in the channel. The related discussion will be given in the subsequent sections. In addition, based on the above analysis, the overall beam domain model can be expressed as

$$\mathbf{H}_B(t, f) = \check{\mathbf{H}}_B(t, f) + \hat{\mathbf{H}}_B(t, f). \quad (29)$$

For the sake of understanding and using the proposed models better, a brief flow chart about how to generate the CTFs of GBSM and BDCM is given in Fig. 4.

IV. STATISTICAL PROPERTIES OF THE PROPOSED GBSM AND BDCM

A. Channel Power

For the proposed BDCM, the total power of the channel can be calculated as

$$\sigma_B^2 = \mathbb{E}(\text{trace}[\mathbf{H}_B^H \mathbf{H}_B]) = \sum_{i'=1}^{K_R L_R} \sum_{j'=1}^{K_T L_T} \mathbb{E}[|h_{i', j'}^B|^2] \quad (30)$$

where $h_{i', j'}^B$ is the element in i' -th row and j' -th column of \mathbf{H}_B , and \mathbb{E} denotes the statistical average. For the sake of conciseness, the variables time and frequency are omitted in the derivations of channel power and several following statistical properties. Under the uncorrelated scattering assumption, the power of the channel elements can be obtained as

$$\mathbb{E}[|h_{i', j'}^B|^2] = \hat{\sigma}_{i', j'}^2 + \check{\sigma}_{i', j'}^2 \quad (31)$$

where $\hat{\sigma}_{i', j'}^2$ and $\check{\sigma}_{i', j'}^2$ represent the power of the clusters under array stationary and non-stationary conditions, respectively, which can be calculated as

$$\hat{\sigma}_{i', j'}^2 \approx \sum_{n \in \mathbf{N}_1(t)} \sum_{m_n=1}^{M_n} P_{m_n}(t) \left| J_0(\tilde{k} \rho_{k_R, l_R}^{R, m_n}(t)) \right|^2 \times \left| J_0(\tilde{k} \rho_{k_T, l_T}^{T, m_n}(t)) \right|^2 \quad (32)$$

$$\begin{aligned} \check{h}_{i', j'}^B(t, f) &= [\tilde{\mathbf{U}}_R^T]_{i', :} \check{\mathbf{H}}(t, f) [\tilde{\mathbf{U}}_T]_{:, j'} \\ &= \sum_{n \in \mathbf{N}_2(t)} \sum_{m_n=1}^{M_n} \sqrt{P_{m_n}(t)} e^{j\Phi_{m_n}} e^{j2\pi(f_c - f)\tau_{m_n}^c(t)} \\ &\quad \times \frac{1}{M_R} \sum_{s_r=1}^{S_r} \sum_{q \in V_{m_n}^{s_r}} e^{j\frac{2\pi}{\lambda} R_r [\sin \tilde{\theta}_{k_R}^R \cos(\tilde{\varphi}_{l_R}^R - \phi_q^R) - \sin \theta_{m_n}^{R, s_r}(t) \cos(\varphi_{m_n}^{R, s_r}(t) - \phi_q^R)]} \\ &\quad \times \frac{1}{M_T} \sum_{s_t=1}^{S_t} \sum_{p \in V_{m_n}^{s_t}} e^{j\frac{2\pi}{\lambda} R_t [\sin \tilde{\theta}_{k_T}^T \cos(\tilde{\varphi}_{l_T}^T - \phi_p^T) - \sin \theta_{m_n}^{T, s_t}(t) \cos(\varphi_{m_n}^{T, s_t}(t) - \phi_p^T)]} \\ &= \sum_{n \in \mathbf{N}_2(t)} \sum_{m_n=1}^{M_n} \sqrt{P_{m_n}(t)} e^{j\Phi_{m_n}} e^{j2\pi(f_c - f)\tau_{m_n}^c(t)} \check{J}_{m_n}^{k_R, l_R}(t) \check{J}_{m_n}^{k_T, l_T}(t) \end{aligned} \quad (26)$$

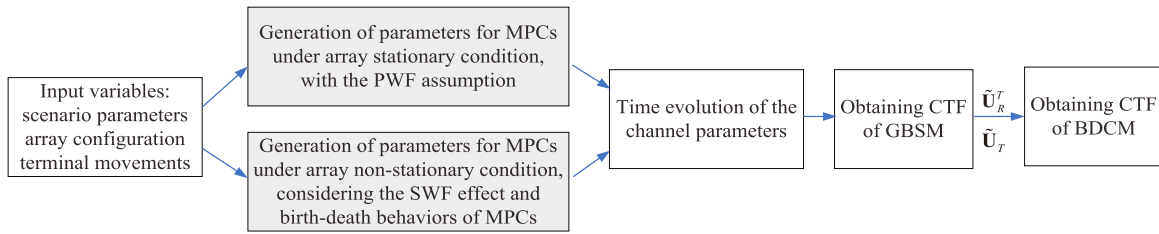


Fig. 4. Flow chart of channel generation procedure.

$$\tilde{\sigma}_{i',j'}^2 = \sum_{n \in \mathbf{N}_2(t)} \sum_{m_n=1}^{M_n} P_{m_n}(t) |\check{J}_{m_n}^{k_R, l_R}(t)|^2 |\check{J}_{m_n}^{k_T, l_T}(t)|^2. \quad (33)$$

In fact, the shapes of $|J_0(\tilde{k}\rho_{k_R, l_R}^{R, m_n}(t))|^2$ and $|J_0(\tilde{k}\rho_{k_T, l_T}^{T, m_n}(t))|^2$ are peaky around k_R -th/ k_T -th and l_R -th/ l_T -th beams and similar to that of the Dirac delta function for sufficiently large antenna numbers. Therefore, the power of MPCs under array stationary condition can be considered to be almost entirely distributed over the corresponding beams with negligible power leakage. In other words, the power on a certain beam is the sum of the power of MPCs that are divided into this beam according to their angles. However, for the MPCs under array non-stationary condition, the superposition of non-zero order Bessel functions will lead to interference with the mutual selection between the beams and the MPCs. In this case, the spatial resolution of the BDCM will decrease and the power of this kind of MPCs will disperse on different beams, causing the inescapable power leakage.

B. Power Leakage

As mentioned in the previous sections, power leakage exists between the beams in BDCM. In fact, the power leakage in the model can be divided into two categories, one from the imperfect beam sampling [46], [47], and the other from power dispersion caused by small VRs and the resulting low spatial resolution [37]. In order to reflect the phenomenon of power leakage clearly, we only consider the case where only one scattering path exists in the channel. Then, the power leakage can be calculated in a simplified way as

$$\eta = 1 - \max_{i',j'}(\mathbb{E}[|h_{i',j'}^B|^2]) \quad (34)$$

where $\max(\cdot)$ indicates the selection of the maximum value.

C. STF-CF

For GBSM, the correlation characteristics between the channel elements $h_{p,q}(t, f)$ and $h_{p',q'}(t + \Delta t, f + \Delta f)$ can be reflected in STF-CF, which can be calculated as

$$\begin{aligned} \kappa_{p,q,p',q'}^G(t, f; \Delta t, \Delta f) &= \mathbb{E}[h_{p,q}(t, f)(h_{p',q'}(t + \Delta t, f + \Delta f))^*] \\ &= \sum_{n=0}^{\mathbf{N}(t)} \sum_{m_n=1}^{M_n} e^{j2\pi(f_c - f)[\tau_{m_n}^c(t) + \tau_{m_n}^{p,q}(t) - \tau_{m_n}^c(t + \Delta t) - \tau_{m_n}^{p',q'}(t + \Delta t)]} \\ &\quad \cdot e^{j2\pi\Delta f[\tau_{m_n}^c(t + \Delta t) + \tau_{m_n}^{p',q'}(t + \Delta t)]} a_{m_n}^{p,q,p',q'}(t, \Delta t) \end{aligned} \quad (35)$$

where $(\cdot)^*$ denotes the complex conjugation operation, Δt and Δf are the time and frequency differences, respectively, $a_{m_n}^{p,q,p',q'}(t, \Delta t) = \eta_{m_n}^{p,q} \eta_{m_n}^{p',q'} \sqrt{P_{m_n}(t)P_{m_n}(t + \Delta t)}$ determines the contribution of the m -th ray in the n -th cluster to the STF-CF.

By replacing the array domain channel elements in (35) with the beam domain channel elements $h_{i',j'}^B(t, f)$ and $h_{i'',j''}^B(t + \Delta t, f + \Delta f)$, the STF-CF of BDCM can be calculated as

$$\begin{aligned} \kappa_{i',j',i'',j''}^B(t, f; \Delta t, \Delta f) &= \mathbb{E}[h_{i',j'}^B(t, f)(h_{i'',j''}^B(t + \Delta t, f + \Delta f))^*] \end{aligned} \quad (36)$$

Considering the uncorrelated scattering environment, $\kappa_{i',j',i'',j''}^B$ can be written as the summation of different components' correlations, i.e.,

$$\begin{aligned} \kappa_{i',j',i'',j''}^B(t, f; \Delta t, \Delta f) &= \hat{\kappa}_{i',j',i'',j''}^B(t, f; \Delta t, \Delta f) \\ &\quad + \check{\kappa}_{i',j',i'',j''}^B(t, f; \Delta t, \Delta f) \end{aligned} \quad (37)$$

where $\hat{\kappa}_{i',j',i'',j''}^B(t, f; \Delta t, \Delta f)$ and $\check{\kappa}_{i',j',i'',j''}^B(t, f; \Delta t, \Delta f)$ can be obtained by substituting (20) and (26) into (36), and are presented in (38) and (39), shown at the bottom of the next page, respectively. In (38) and (39), $k_R' = \lceil \frac{i''}{L_R} \rceil$, $l_R' = i'' - (k_R' - 1)L_R$, $k_T' = \lceil \frac{j''}{L_T} \rceil$, and $l_T' = j'' - (k_T' - 1)L_T$ are the beams corresponding to $h_{i'',j''}^B(t + \Delta t, f + \Delta f)$. As previously stated, the beamwidths of the MPCs under array non-stationary condition will increase due to the superposition of non-zero order Bessel functions, which will introduce higher correlation between this kind of channel elements.

D. Beam Spread

To describe the power dispersion of BDCM, beam spread is adopted [37]. The calculation method of beam spread is similar to angular spread. For example, the azimuth beam spread at Rx side can be expressed as

$$\zeta_A^R(t) = \sqrt{\tilde{\varphi}_R^2 - \tilde{\varphi}_R'^2} \quad (40)$$

where

$$\tilde{\varphi}_R^2 = \sum_{l_R=1}^{L_R} \sum_{k_R=1}^{K_R} \sum_{j'=1}^{K_T L_T} |h_{i',j'}^B|^2 (\tilde{\varphi}_{l_R}^R)^2 / \sum_{i'=1}^{K_R L_R} \sum_{j'=1}^{K_T L_T} |h_{i',j'}^B|^2 \quad (41)$$

$$\tilde{\varphi}_R' = \sum_{l_R=1}^{L_R} \sum_{k_R=1}^{K_R} \sum_{j'=1}^{K_T L_T} |h_{i',j'}^B|^2 \tilde{\varphi}_{l_R}^R / \sum_{i'=1}^{K_R L_R} \sum_{j'=1}^{K_T L_T} |h_{i',j'}^B|^2 \quad (42)$$

where i' in the numerator of (41) and (42) is determined according to l_R and k_R . The zenith beam spread at Rx side can

be obtained by replacing $\tilde{\varphi}_{l_R}^R$ with $\tilde{\theta}_{k_R}^R$ and the azimuth/zenith beam spreads at Tx side can be obtained in the similar way. It should be noticed that the degree of the power leakage associated with the VRs and the array antenna numbers will affect the characterization of the power dispersion of MPCs in 3-D space.

V. RESULTS AND ANALYSIS

In this section, the statistical properties are simulated and the corresponding discussions are given. Furthermore, a comparison of some channel characteristics in array domain and beam domain is provided. In the maritime communication scenarios, two kinds of clusters exist besides the LoS path, i.e., scattering clusters from evaporation duct propagation and scattering clusters caused by rough sea surface. In the simulation, the LoS path is neglected to ensure that the channel properties can be clearly observed. Besides, to better embody the small-scale properties, the large-scale fading is normalized in the following simulation results. Unless otherwise specified, all the simulation results are obtained at the Rx side and the following simulation parameters are consistent in all statistical property simulations: $f_c = 5.8$ GHz, $M_R = 256$, $S_r = 4$, $M_T = 1$, $S_t = 1$, $d_r = d_t = \lambda/2$, $\tilde{\lambda}^R = 0.103$, and $\tilde{\lambda}_M^R = 4.07$ [24]. Other specific simulation parameters can refer to [29]. In the simulation, the proportion of clusters that undergo the array non-stationary process is described by the coefficient γ and the single antenna assumption of Tx is adopted to improve simulation efficiency.

Fig. 5 visualizes the normalized power of the channel elements in the proposed BDCM and the channel power of BDCM can be found to be sparse. The sparsity of the beam domain channel elements can offer significant benefits for reducing the computational complexity of transmission schemes. In Fig. 5(a), the power of channel elements at initial moment t_0 is obtained under the array domain wide sense stationary (WSS) assumption. This assumption ignores the near-field effect and assumes all the clusters are under array stationary condition, i.e., $\gamma = 0$. The beam with higher power in the bottom-right corner of Fig. 5(a) shows the presence of the scattering clusters from evaporation duct propagation, which are more concentrated due to the smaller angular spread. In comparison, the angles of scattering clusters caused by the sea surface fluctuations are more dispersed. Hence multiple beams with slightly lower power can be observed. The channel element power shown in Fig. 5(b) is generated with $\gamma \neq 0$, i.e., the near-field effect of the clusters which are under array non-

stationary condition is considered. In fact, due to the large distances of the evaporation duct clusters from the antenna arrays, almost all evaporation duct clusters are in the far-field range, and only part of the sea surface clusters' array non-stationarities need to be considered. The ratio of array non-stationary clusters to all clusters γ can be adjusted according to specific scenarios. In our simulation, the statistical average of γ at different time instants is around 0.53. In Fig. 5(a), the interaction between the MPCs is weak due to the high spatial resolution. Intuitively, it appears that the number of clusters in Fig. 5(b) is reduced in comparison with that in Fig. 5(a). But in reality this is due to the dispersion of cluster power, which reduces the relative power of the clusters with small VRs. Therefore, such clusters become relatively insignificant in Fig. 5(b). To illustrate the dispersion of power caused by the decrease in spatial resolution more specifically, the normalized power of the channel elements in $\tilde{\mathbf{H}}_B$ is shown separately in Fig. 5(c). It can be found that some clusters cannot be well resolved and their power is diffused over many beams. Therefore, the interaction between the MPCs with small VRs is introduced into the beam domain channel, making multipath fading non-negligible. As the antenna position shifts and the maritime environment changes, some old clusters will disappear and some new clusters will arise at different time instants, which leads to the time non-stationarity. In Fig. 5(d), the normalized channel power for the time instant $t = t_0 + 5$ s is presented to show the time non-stationarity of the channel model. From Fig. 5(d), the birth-death process of clusters in the time domain can be observed.

Fig. 6 shows the power leakage with different antenna array sizes. The simulation is carried out by taking the numbers of antennas with interval of 32. Here, it is assumed that there is no array non-stationary phenomenon on the array, and the VR of the cluster can cover the whole array. From Fig. 6, it can be found that the variation of power leakage with increasing number of antennas is not monotonic, which may be caused by the narrower beamwidth and the deviations between beam samplings and the AoAs of MPCs. Because the number of beam samplings is related to the array size, the number of antennas in the array will affect the beam division and thus has an influence on the power leakage. Fig. 7 illustrates the effect of the VR size on power leakage in BDCM. Three arrays of different antenna numbers are used in the simulation to explore the impact of the total number of antennas on power leakage for a given number of visible antennas. As the number of visible antennas increases, a decreasing trend in

$$\begin{aligned} \tilde{k}_{i',j',i'',j''}^B(t, f; \Delta t, \Delta f) &\approx \sum_{n \in \mathbf{N}_1(t)} \sum_{m_n=1}^{M_n} \sqrt{P_{m_n}(t)P_{m_n}(t+\Delta t)} e^{j2\pi(f_c-f)[\tau_{m_n}^c(t)-\tau_{m_n}^c(t+\Delta t)]} \\ &\times e^{j2\pi\Delta f\tau_{m_n}^c(t+\Delta t)} \times J_0(\tilde{k}_{k_R,l_R}^{R,m_n}(t)) J_0(\tilde{k}_{k_T,l_T}^{T,m_n}(t)) J_0(\tilde{k}_{k_R',l_R'}^{R,m_n}(t+\Delta t)) J_0(\tilde{k}_{k_T',l_T'}^{T,m_n}(t+\Delta t)) \end{aligned} \quad (38)$$

$$\begin{aligned} \tilde{k}_{i',j',i'',j''}^B(t, f; \Delta t, \Delta f) &= \sum_{n \in \mathbf{N}_2(t)} \sum_{m_n=1}^{M_n} \sqrt{P_{m_n}(t)P_{m_n}(t+\Delta t)} e^{j2\pi(f_c-f)[\tau_{m_n}^c(t)-\tau_{m_n}^c(t+\Delta t)]} \\ &\times e^{j2\pi\Delta f\tau_{m_n}^c(t+\Delta t)} \times \check{J}_{m_n}^{k_R,l_R}(t) \check{J}_{m_n}^{k_T,l_T}(t) (\check{J}_{m_n}^{k_R',l_R'}(t+\Delta t))^* (\check{J}_{m_n}^{k_T',l_T'}(t+\Delta t))^* \end{aligned} \quad (39)$$

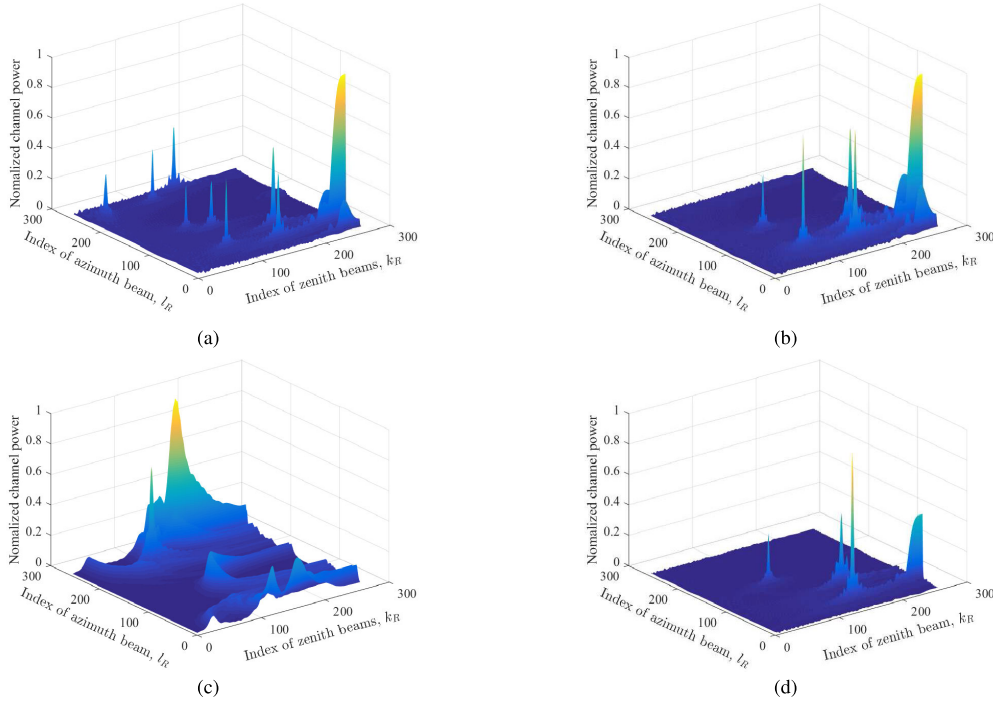


Fig. 5. The normalized channel power under different time instants and array domain WSS/non-WSS assumptions: (a) Power of channel elements in \mathbf{H}_B , $t = t_0$ s, $\gamma = 0$, (b) Power of channel elements in \mathbf{H}_B , $t = t_0$ s, $\gamma \neq 0$, (c) Power of channel elements in $\tilde{\mathbf{H}}_B$, $t = t_0$ s, $\gamma \neq 0$, (d) Power of channel elements in \mathbf{H}_B , $t = t_0 + 5$ s, $\gamma \neq 0$.

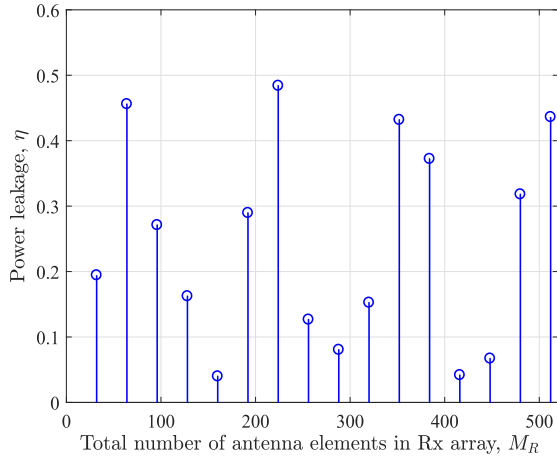


Fig. 6. The power leakage at different antenna array sizes under array domain WSS assumption.

power leakage can be seen. Besides, with the same number of visible antennas, the less the total number of antennas, the faster the power leakage drops. The reason behind this is that the larger the proportion of the visible antenna number to the total antenna number, the narrower the beamwidth, and the lower the power leakage. This result means that the ratio of the visible antenna number to the total antenna number is a key factor in determining power leakage.

The comparison of the spatial CFs (SCFs) for the BDCMs under array domain WSS and non-WSS assumptions are given in Fig. 8. To be succinct, only the correlation matrices of azimuth beams, which are obtained by adding up the correlations on all corresponding zenith beams with $\Delta t = \Delta f = 0$, are discussed here. Fig. 8(a) is obtained with $\gamma = 0$, which means the array non-stationarity is not regarded. While in Fig. 8(b), the clusters in the near-field range show the

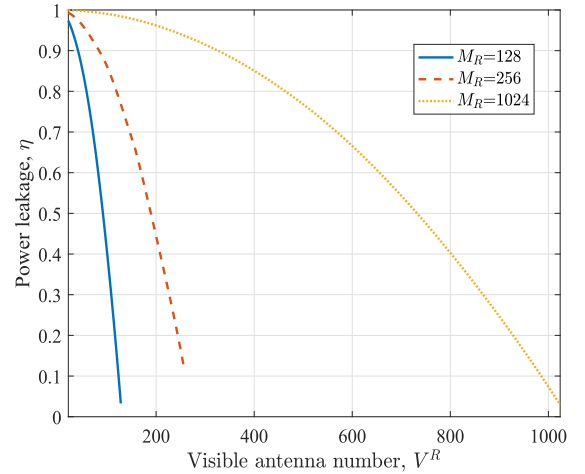


Fig. 7. The power leakage with the varying number of visible antennas at different total numbers of antennas.

evolution process on the array. As shown in these two figures, the elements near the diagonal have relatively large values, i.e., the adjacent beams show relatively large correlation. From the comparison of the parts framed by rectangles, the correlation of these channel elements in Fig. 8(b) become low, which may be caused by the power reduction resulting from the small VRs of the corresponding clusters. As illustrated in the parts framed by the ellipses, the correlation of nearby beams become higher, which is caused by the power dispersion of the clusters that have large VRs. Besides, it can be found that the correlations of beams are related to the AoAs of MPCs, which implies the channel is not WSS in beam domain. Furthermore, it can be inferred from the comparison that the channel non-stationarity in the array domain can further trigger the channel non-stationarity in the beam domain, which is caused by the dispersion of cluster power over the beams.

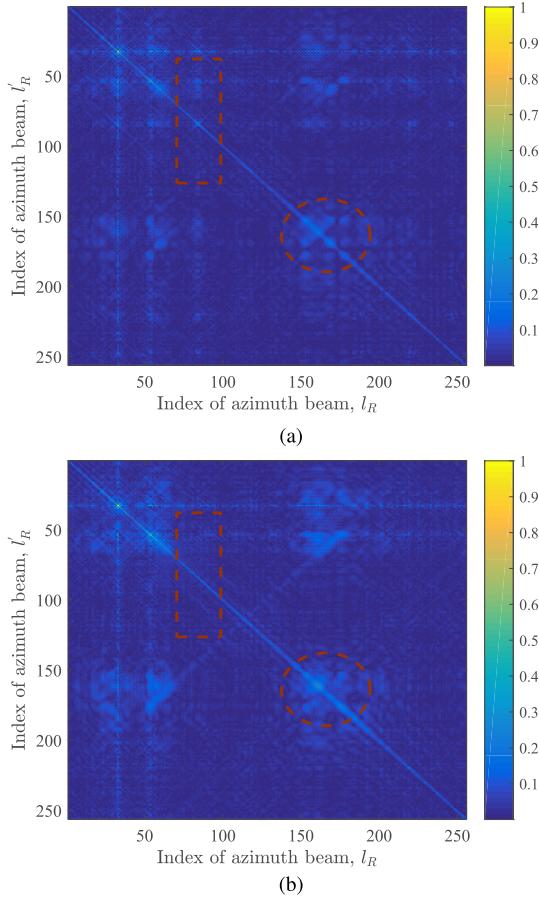


Fig. 8. The normalized SCFs of the proposed BDCM: (a) $\gamma = 0$, (b) $\gamma \neq 0$.

This phenomenon indicates that the GBSM and BDCM are internally consistent in terms of spatial stationarity.

In Fig. 9, the frequency CFs (FCFs) of the proposed GBSM and BDCM are presented. The simulation result of BDCM shows the correlations calculated directly from the definition, while the analytical result of BDCM is obtained from the detailed derivation of (37) with the approximation using Bessel functions. The good match of the two kinds of curves proves the reasonableness of the approximation. Similarly, the correctness of the simulations and derivations can be verified by the consistency between the analytical result and simulation result of GBSM FCF. As shown in Fig. 9, the fluctuation in frequency correlation of BDCM is smaller than that of GBSM, i.e., the frequency response of BDCM is flatter. The reason behind this may be that the correlation of a certain cluster corresponding to the beam takes the dominant role, which weakens the influence of other clusters so that the frequency correlation does not change much.

The effects of array non-stationarity and array size on the temporal autocorrelation functions (ACFs) of the proposed GBSM and BDCM are reflected in Fig. 10. As shown in Fig. 10, both the ACF curves of the GBSM and BDCM are affected by power distribution changes of array non-stationary clusters on the antennas and beams. Moreover, the beam domain channel changes more slowly. Meanwhile, the influence of different array antenna numbers on the ACF curves of BDCM is investigated. The beams selected for comparison under different antenna sizes represent similar

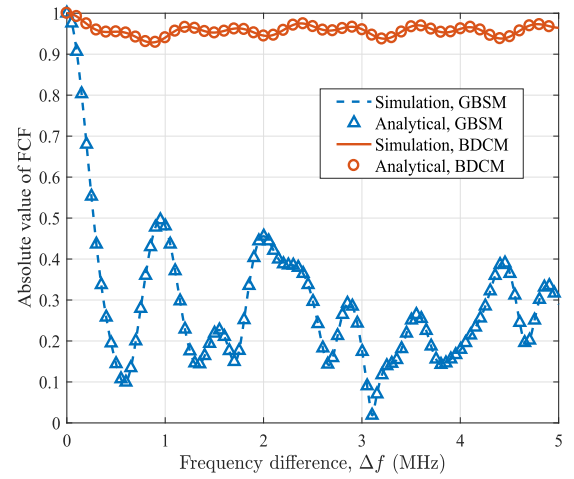


Fig. 9. The normalized FCFs of the proposed GBSM and BDCM.

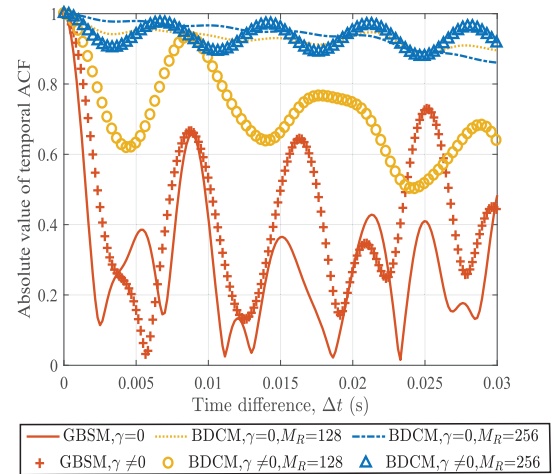


Fig. 10. The normalized temporal ACFs of the proposed GBSM and BDCM.

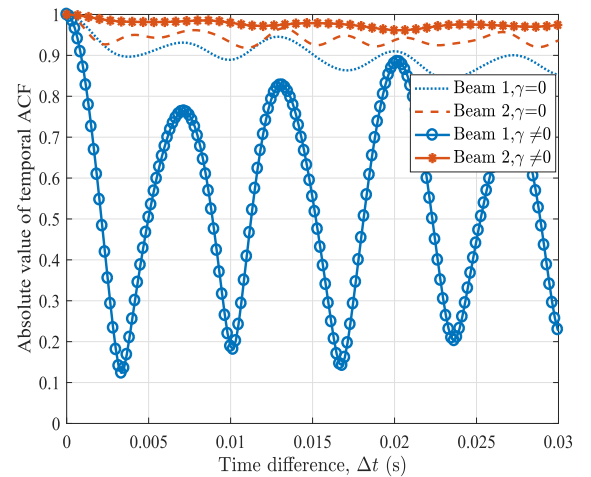


Fig. 11. The normalized temporal ACFs of the beams corresponding to different kinds of clusters.

ranges in the angle domain. When the number of antennas is higher, the beamwidth becomes narrower and the dominant path effect is stronger, so that the correlation changes less both when the WSS assumption in array domain holds or not. In Fig. 11, the maritime channel characteristics in the beam domain can be reflected. Beam 1 stands for the beam corresponding to a sea surface cluster, which is in the near-field range and experiences the array evolution process

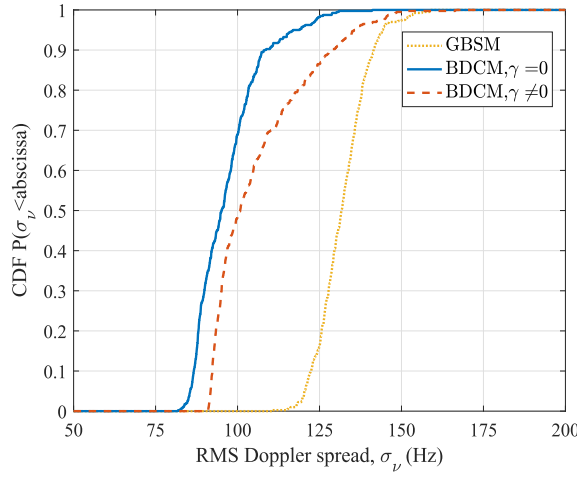


Fig. 12. Doppler spreads of the proposed GBSM and BDCM under array domain WSS and non-WSS assumptions.

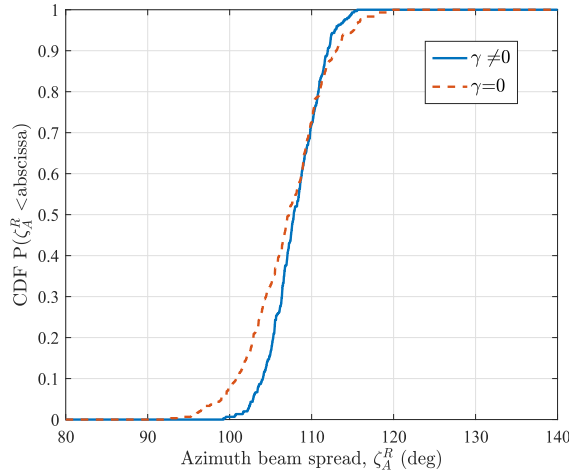


Fig. 13. Azimuth beam spreads of the proposed BDCM under array domain WSS and non-WSS assumptions.

when considering the non-stationarity in the array domain. Therefore, this path becomes less dominant, which makes the ACF curve change rapidly. Beam 2 stands for the beam to which the clusters from evaporation duct propagation belong, and the clusters are almost all in the far-field range. The reason for the increase in correlation after considering the array non-stationarity may lie in the diminished impact of the clusters belonging to the surrounding beams.

In Fig. 12, the cumulative distribution function (CDF) curves of the RMS Doppler spreads for the proposed GBSM and BDCM are compared. The Doppler spread of GBSM is obtained under the array domain WSS assumption and is larger than that of the BDCM. Because the Doppler spread of BDCM is obtained for one of the beams, which means that only the Doppler frequencies of clusters within the beam range affect the simulation results. When the array non-stationarity is considered in the BDCM, the value of Doppler spread will increase. Fig. 13 illustrates the azimuth beam spreads at the Rx side. Similarly, the array non-stationarity leads to dispersion of cluster power on the beams, resulting in changes of beam spread. According to the simulation results, it can be known that the array non-stationarity cannot be ignored in order to obtain accurate beam domain channel characteristics.

VI. CONCLUSION

In this paper, we have proposed a 3-D non-stationary massive MIMO GBSM and a corresponding BDCM for maritime communication systems using UCAs. In the proposed BDCM, the appropriate beamforming matrices have been adopted to transform the corresponding GBSM from the array domain to the beam domain and the proof of their invertibility has been given. By introducing the VR method into the proposed GBSM/BDCM and dividing UCAs into sub-arrays, the array non-stationarity in massive MIMO channels has been characterized. Statistical properties of both models including channel power, power leakage, STF-CF, and RMS Doppler/beam spreads have been derived and simulated, and the influence of the array non-stationarity on statistical properties has been explored. According to the derivation and simulation results, it can be concluded that the array non-stationarity greatly affects the characteristics of maritime massive MIMO channels and therefore cannot be ignored in the modeling effort. In addition, compared with the GBSM, the corresponding BDCM presents sparsity in terms of the channel matrix and therefore is more insensitive to the Doppler effect, which can give insights to the design of beam domain transmission schemes in maritime communications.

APPENDIX A

For the sake of convenience, we rewrite (20) as

$$\hat{h}_{i',j'}^B(t, f) = \sum_{n \in \mathbf{N}_1(t)} \sum_{m_n=1}^{M_n} \sqrt{P_{m_n}(t)} e^{j\Phi_{m_n}} e^{j2\pi(f_c - f)\tau_{m_n}^c(t)} \cdot \hat{I}_{k_R, l_R}^{R, m_n}(t) \cdot \hat{I}_{k_T, l_T}^{T, m_n}(t) \quad (43)$$

with

$$\hat{I}_{k_R, l_R}^{R, m_n}(t) = \frac{1}{M_R} \sum_{q=1}^{M_R} e^{j\tilde{k}_R \sin \tilde{\theta}_{k_R}^R \cos(\tilde{\varphi}_{l_R}^R - \phi_q^R)} \cdot e^{-j\tilde{k}_R \sin \theta_{m_n}^R(t) \cos(\varphi_{m_n}^R(t) - \phi_q^R)} \quad (44)$$

$$\hat{I}_{k_T, l_T}^{T, m_n}(t) = \frac{1}{M_T} \sum_{p=1}^{M_T} e^{j\tilde{k}_T \sin \tilde{\theta}_{k_T}^T \cos(\tilde{\varphi}_{l_T}^T - \phi_p^T)} \cdot e^{-j\tilde{k}_T \sin \theta_{m_n}^T(t) \cos(\varphi_{m_n}^T(t) - \phi_p^T)} \quad (45)$$

The definitions of the variables $\xi_{k_R, l_R}^{R, m_n}(t)$ and $\xi_{k_T, l_T}^{T, m_n}(t)$ are given in (46) and (47), shown at the bottom of the next page. By combining (21), (44), and (46), $\hat{I}_{k_R, l_R}^{R, m_n}(t)$ can be reduced as

$$\hat{I}_{k_R, l_R}^{R, m_n}(t) = \frac{1}{M_R} \sum_{q=1}^{M_R} e^{j\tilde{k}_R \rho_{k_R, l_R}^{R, m_n}(t) \cos(\xi_{k_R, l_R}^{R, m_n}(t) - \phi_q^R)} \stackrel{(c_1)}{=} \sum_{a=-\infty}^{\infty} e^{jaM_R(\pi/2 - \xi_{k_R, l_R}^{R, m_n}(t))} J_{aM_R}(\tilde{k}_R \rho_{k_R, l_R}^{R, m_n}(t)) \quad (48)$$

where c_1 holds because the antenna elements in the array are angular symmetric, i.e., $\phi_q^R = 2\pi(q-1)/M_R$ [42]. In fact, the zero order Bessel function $J_0(\cdot)$ is the principal term of $\hat{I}_{k_R, l_R}^{R, m_n}$ [12]. Therefore, when the number of the antennas

elements is sufficiently large, $\hat{I}_{k_R, l_R}^{R, m_n}(t)$ can be approximated as

$$\hat{I}_{k_R, l_R}^{R, m_n}(t) \approx J_0(\tilde{k}\rho_{k_R, l_R}^{R, m_n}(t)). \quad (49)$$

Through a similar process, $\hat{I}_{k_T, l_T}^{T, m_n}(t)$ can be approximated as

$$\hat{I}_{k_T, l_T}^{T, m_n}(t) \approx J_0(\tilde{k}\rho_{k_T, l_T}^{T, m_n}(t)). \quad (50)$$

By substituting (49) and (50) into (43), (20) can be obtained.

Similar to (43), the channel element of the BDCM under array non-stationary condition in (26) can be rewritten as

$$\tilde{h}_{i', j'}^B(t, f) = \sum_{n \in \mathbf{N}_2(t)} \sum_{m_n=1}^{M_n} \sqrt{P_{m_n}(t)} e^{j\Phi_{m_n}} e^{j2\pi(f_c - f)\tau_{m_n}^c(t)} \cdot \check{I}_{k_R, l_R}^{R, m_n}(t) \cdot \check{I}_{k_T, l_T}^{T, m_n}(t) \quad (51)$$

with

$$\check{I}_{k_R, l_R}^{R, m_n}(t) = \frac{1}{M_R} \sum_{s_r=1}^{S_r} \sum_{q=q_{s_r, s_r}^{m_n}}^{q_{e, s_r}^{m_n}} e^{j\tilde{k}R_r \sin \tilde{\theta}_{k_R}^R \cos(\tilde{\varphi}_{l_R}^R - \phi_q^R)} \cdot e^{-j\tilde{k}R_r \sin \theta_{m_n}^{R, s_r}(t) \cos(\varphi_{m_n}^{R, s_r}(t) - \phi_q^R)} \quad (52)$$

$$\check{I}_{k_T, l_T}^{T, m_n}(t) = \frac{1}{M_T} \sum_{s_t=1}^{S_t} \sum_{p=p_{s_t, s_t}^{m_n}}^{p_{e, s_t}^{m_n}} e^{j\tilde{k}R_t \sin \tilde{\theta}_{k_T}^T \cos(\tilde{\varphi}_{l_T}^T - \phi_p^T)} \cdot e^{-j\tilde{k}R_t \sin \theta_{m_n}^{T, s_t}(t) \cos(\varphi_{m_n}^{T, s_t}(t) - \phi_p^T)} \quad (53)$$

where $\{q_{s_r, s_r}^{m_n}, p_{s_t, s_t}^{m_n}\}$ and $\{q_{e, s_r}^{m_n}, p_{e, s_t}^{m_n}\}$ are the start and end indexes for the antenna elements in $V_{m_n}^{R, s_r}$ and $V_{m_n}^{T, s_t}$, respectively. By combining (21), (46), and (52), $\check{I}_{k_R, l_R}^{R, m_n}(t)$ can be reduced as

$$\begin{aligned} \check{I}_{k_R, l_R}^{R, m_n}(t) &= \frac{1}{M_R} \sum_{s_r=1}^{S_r} \sum_{q=q_{s_r, s_r}^{m_n}}^{q_{e, s_r}^{m_n}} e^{j\tilde{k}\rho_{k_R, l_R}^{s_r, m_n}(t) \cos(\xi_{k_R, l_R}^{s_r, m_n}(t) - \phi_q^R)} \\ &= \frac{1}{M_R} \sum_{s_r=1}^{S_r} \sum_{a=-\infty}^{\infty} e^{ja(\pi/2 - \xi_{k_R, l_R}^{s_r, m_n}(t))} \\ &\quad \times J_a(\tilde{k}\rho_{k_R, l_R}^{s_r, m_n}(t)) \sum_{q=q_{s_r, s_r}^{m_n}}^{q_{e, s_r}^{m_n}} e^{ja\phi_q^R} \\ &= \sum_{s_r=1}^{S_r} \sum_{a=-\infty}^{\infty} e^{ja(\pi/2 - \xi_{k_R, l_R}^{s_r, m_n}(t))} J_a(\tilde{k}\rho_{k_R, l_R}^{s_r, m_n}(t)) f_{m_n}^{s_r}(a) \\ &= \check{J}_{m_n}^{k_R, l_R}(t) \end{aligned} \quad (54)$$

where $\rho_{k_R, l_R}^{s_r, m_n}(t)$ and $\xi_{k_R, l_R}^{s_r, m_n}(t)$ can be obtained by replacing $\theta_{m_n}^R(t)$ and $\varphi_{m_n}^R(t)$ in (21) and (46) with $\theta_{m_n}^{R, s_r}(t)$ and

$\varphi_{m_n}^{R, s_r}(t)$, and $f_{m_n}^{s_r}(a)$ can be expressed as

$$f_{m_n}^{s_r}(a) = e^{j\pi a(q_{e, s_r}^{m_n} + q_{s_r, s_r}^{m_n} - 2)/M_R} \cdot \frac{\sin[\pi a(q_{e, s_r}^{m_n} - q_{s_r, s_r}^{m_n} + 1)/M_R]}{M_R \sin(\pi a/M_R)}. \quad (55)$$

Similarly, $\check{I}_{k_T, l_T}^{T, m_n}(t)$ can be expressed as

$$\check{I}_{k_T, l_T}^{T, m_n}(t) = \sum_{s_t=1}^{S_t} \sum_{b=-\infty}^{\infty} e^{jb(\pi/2 - \xi_{k_T, l_T}^{s_t, m_n}(t))} J_b(\tilde{k}\rho_{k_T, l_T}^{s_t, m_n}(t)) f_{m_n}^{s_t}(b) = \check{J}_{m_n}^{k_T, l_T}(t) \quad (56)$$

where $\rho_{k_T, l_T}^{s_t, m_n}(t)$ and $\xi_{k_T, l_T}^{s_t, m_n}(t)$ can be obtained by replacing $\theta_{m_n}^T(t)$ and $\varphi_{m_n}^T(t)$ in (22) and (47) with $\theta_{m_n}^{T, s_t}(t)$ and $\varphi_{m_n}^{T, s_t}(t)$, and $f_{m_n}^{s_t}(b)$ can be calculated as

$$f_{m_n}^{s_t}(b) = e^{j\pi b(p_{e, s_t}^{m_n} + p_{s_t, s_t}^{m_n} - 2)/M_T} \cdot \frac{\sin[\pi b(p_{e, s_t}^{m_n} - p_{s_t, s_t}^{m_n} + 1)/M_T]}{M_T \sin(\pi b/M_T)}. \quad (57)$$

APPENDIX B

Here, we take $\tilde{\mathbf{U}}_R$ as an example and the invertibility of $\tilde{\mathbf{U}}_T$ can be proved in a similar way. The k_R -th azimuth beamforming matrix $\tilde{\mathbf{U}}_R^{(k_R)}$ in $\tilde{\mathbf{U}}_R$ can be written in the expanded form as (58), shown at the top of the next page, where $b_{k_R} = \frac{2\pi}{\lambda} R_r \sin \tilde{\theta}_{k_R}^R$ is expressed as a coefficient to simplify the equation.

From (58), it can be found that $\tilde{\mathbf{U}}_R^{(k_R)}$ is a circulant Toeplitz matrix when $L_R = M_R$ holds. Then, the matrix can be directly diagonalized by using Fourier transform matrix [15], i.e.,

$$\mathbf{\Lambda}_R^{(k_R)} = \mathbf{A}_R^H \tilde{\mathbf{U}}_R^{(k_R)} \mathbf{A}_R \quad (59)$$

where $\mathbf{A}_R \in \mathbb{C}^{M_R \times M_R}$ is the Fourier transform matrix whose (l, k) -th $(l, k = 1, \dots, M_R)$ entry can be expressed as $[\mathbf{A}_R]_{l, k} = (1/\sqrt{M_R}) \cdot e^{-j2\pi(l-1)(k-1)/M_R}$, and $\mathbf{\Lambda}_R^{(k_R)}$ is a diagonal matrix. Based on (59), the i -th diagonal entry of $\mathbf{\Lambda}_R^{(k_R)}$ [48] can be expressed as

$$\begin{aligned} [\mathbf{\Lambda}_R^{(k_R)}]_{i, i} &= \sum_{l=1}^{M_R} \sum_{k=1}^{M_R} [\mathbf{A}_R^H]_{i, l} [\tilde{\mathbf{U}}_R^{(k_R)}]_{l, k} [\mathbf{A}_R]_{k, i} \\ &= \frac{1}{M_R} \sum_{l=1}^{M_R} \sum_{k=1}^{M_R} e^{-\frac{j2\pi(k-l)(i-1)}{M_R}} e^{jb_{k_R} \cos\left(\frac{2\pi(k-l)}{M_R}\right)} \\ &\quad \stackrel{l'=k-l}{=} \sum_{l'=1}^{M_R} e^{-\frac{j2\pi l'(i-1)}{M_R}} e^{jb_{k_R} \cos\left(\frac{2\pi l'}{M_R}\right)} \\ &= \sum_{l'=0}^{M_R-1} e^{-\frac{j2\pi l'(i-1)}{M_R}} e^{jb_{k_R} \cos\left(\frac{2\pi l'}{M_R}\right)}. \end{aligned} \quad (60)$$

$$\cos \xi_{k_R, l_R}^{R, m_n}(t) = \frac{\sin \tilde{\theta}_{k_R}^R \cos \tilde{\varphi}_{l_R}^R - \sin \theta_{m_n}^R(t) \cos \varphi_{m_n}^R(t)}{\left[\left(\sin \tilde{\theta}_{k_R}^R \cos \tilde{\varphi}_{l_R}^R - \sin \theta_{m_n}^R(t) \cos \varphi_{m_n}^R(t) \right)^2 + \left(\sin \tilde{\theta}_{k_R}^R \sin \tilde{\varphi}_{l_R}^R - \sin \theta_{m_n}^R(t) \sin \varphi_{m_n}^R(t) \right)^2 \right]^{1/2}} \quad (46)$$

$$\cos \xi_{k_T, l_T}^{T, m_n}(t) = \frac{\sin \tilde{\theta}_{k_T}^T \cos \tilde{\varphi}_{l_T}^T - \sin \theta_{m_n}^T(t) \cos \varphi_{m_n}^T(t)}{\left[\left(\sin \tilde{\theta}_{k_T}^T \cos \tilde{\varphi}_{l_T}^T - \sin \theta_{m_n}^T(t) \cos \varphi_{m_n}^T(t) \right)^2 + \left(\sin \tilde{\theta}_{k_T}^T \sin \tilde{\varphi}_{l_T}^T - \sin \theta_{m_n}^T(t) \sin \varphi_{m_n}^T(t) \right)^2 \right]^{1/2}} \quad (47)$$

$$\tilde{\mathbf{U}}_R^{(k_R)} = \begin{bmatrix} e^{jb_{k_R}} & \dots & e^{jb_{k_R} \cos(\frac{2\pi(l_R-1)}{M_R})} & \dots & e^{jb_{k_R} \cos(\frac{2\pi(L_R-1)}{M_R})} \\ \vdots & \ddots & \vdots & \ddots & \vdots \\ e^{jb_{k_R} \cos(\frac{2\pi(1-q)}{M_R})} & \dots & e^{jb_{k_R} \cos(\frac{2\pi(l_R-q)}{M_R})} & \dots & e^{jb_{k_R} \cos(\frac{2\pi(L_R-q)}{M_R})} \\ \vdots & \ddots & \vdots & \ddots & \vdots \\ e^{jb_{k_R} \cos(\frac{2\pi(1-M_R)}{M_R})} & \dots & e^{jb_{k_R} \cos(\frac{2\pi(L_R-M_R)}{M_R})} & \dots & e^{jb_{k_R} \cos(\frac{2\pi(L_R-M_R)}{M_R})} \end{bmatrix} \quad (58)$$

Then, the i -th ($i = 1, \dots, M_R$) singular value of $\tilde{\mathbf{U}}_R^{(k_R)}$ can be obtained from the i -th diagonal entry of $\Lambda_R^{(k_R)}$ [48], i.e.,

$$\mu_i^R(b_{k_R}) = \left| \left[\Lambda_R^{(k_R)} \right]_{i,i} \right|. \quad (61)$$

According to *Lemma 1* and *Theorem 2* in [15], the property of the singular values can be presented as

$$\mu_i^R(b_{k_R}) \stackrel{(c_2)}{=} \mu_{M_R+2-i}^R(b_{k_R}) \stackrel{(c_3)}{=} M_R |J_{i-1}(b_{k_R})| \quad (62)$$

where (c_2) and (c_3) hold when the number of antennas is sufficiently large. Besides, (c_2) is only applicable when $i > 2$ and shows that the singular values of $\tilde{\mathbf{U}}_R^{(k_R)}$ are symmetric.

It should be noted that the singular values of $\tilde{\mathbf{U}}_R^{(k_R)}$ are dependent on the value of b_{k_R} . Considering the effect of zenith beams, the values of b_{k_R} are taken discretely in the range $[0, \frac{2\pi}{\lambda} R_r]$ for different $\tilde{\mathbf{U}}_R^{(k_R)}$. By changing the number of zenith beams, the values of b_{k_R} can be varying, making it possible for b_{k_R} to take any value in the range $[0, \frac{2\pi}{\lambda} R_r]$. Based on the symmetry and finiteness of the singular values, we can deduce that there must exist a value of b_{k_R} such that the values of the Bessel functions at b_{k_R} for 0 to $(M_R - 1)$ -th orders are not 0, which means that the singular values of the corresponding $\tilde{\mathbf{U}}_R^{(k_R)}$ are all non-zero and therefore $\tilde{\mathbf{U}}_R^{(k_R)}$ is row full rank matrix. In this case, the probability of the existence of a right inverse for $\tilde{\mathbf{U}}_R$ can be considered as 1.

REFERENCES

- [1] C. X. Wang, J. Huang, H. Wang, X. Gao, X. You, and Y. Hao, "6G wireless channel measurements and models: Trends and challenges," *IEEE Veh. Technol. Mag.*, vol. 15, no. 4, pp. 22–32, Dec. 2020.
- [2] X. You et al., "Towards 6G wireless communication networks: Vision, enabling technologies, and new paradigm shifts," *Sci. China Inf. Sci.*, vol. 64, no. 1, pp. 110301–110374, Jan. 2021.
- [3] C.-X. Wang, Z. Lv, X. Gao, X. You, Y. Hao, and H. Haas, "Pervasive wireless channel modeling theory and applications to 6G GBSMs for all frequency bands and all scenarios," *IEEE Trans. Veh. Technol.*, vol. 71, no. 9, pp. 9159–9173, Sep. 2022.
- [4] J. Wang et al., "Wireless channel models for maritime communications," *IEEE Access*, vol. 6, pp. 68070–68088, 2018.
- [5] Y. Liu, C.-X. Wang, H. Chang, Y. He, and J. Bian, "A novel non-stationary 6G UAV channel model for maritime communications," *IEEE J. Sel. Areas Commun.*, vol. 39, no. 10, pp. 2992–3005, Oct. 2021.
- [6] C. F. Lopez and C.-X. Wang, "A study of 2D non-stationary massive MIMO channels by transformation of delay and angular power spectral densities," *IEEE Trans. Veh. Technol.*, vol. 69, no. 12, pp. 14212–14224, Dec. 2020.
- [7] S. A. Busari, K. M. S. Huq, S. Mumtaz, L. Dai, and J. Rodriguez, "Millimeter-wave massive MIMO communication for future wireless systems: A survey," *IEEE Commun. Surveys Tuts.*, vol. 20, no. 2, pp. 836–869, 2nd Quart., 2018.
- [8] C. F. Lopez, C.-X. Wang, and Y. Zheng, "A 3D non-stationary wideband massive MIMO channel model based on ray-level evolution," *IEEE Trans. Commun.*, vol. 70, no. 1, pp. 621–634, Jan. 2022.
- [9] J. Wang, C.-X. Wang, J. Huang, H. Wang, and X. Gao, "A general 3D space-time-frequency non-stationary THz channel model for 6G ultra-massive MIMO wireless communication systems," *IEEE J. Sel. Areas Commun.*, vol. 39, no. 6, pp. 1576–1589, Jun. 2021.
- [10] J. H. Laarhuis, "MaritimeMaNet: Mobile ad-hoc networking at sea," in *Proc. Int. WaterSide Secur. Conf.*, Nov. 2010, pp. 1–6.
- [11] M. Manoufali, P.-Y. Kong, and S. Jimaa, "An overview of maritime wireless mesh communication technologies and protocols," *Int. J. Bus. Data Commun. Netw.*, vol. 10, no. 1, pp. 1–29, Jan. 2014.
- [12] C. Balannis, *Antenna Theory-Analysis Design*. 2nd ed. Hoboken, NJ, USA: Wiley, 1997.
- [13] W. Fan, I. Carton, J. Ø. Nielsen, K. Olesen, and G. F. Pedersen, "Measured wideband characteristics of indoor channels at centimetric and millimetric bands," *EURASIP J. Wireless Commun. Netw.*, vol. 2016, no. 1, pp. 1–13, 2016.
- [14] P. Ioannides and C. A. Balanis, "Uniform circular and rectangular arrays for adaptive beamforming applications," *IEEE Antennas Wireless Propag. Lett.*, vol. 4, pp. 351–354, 2005.
- [15] P. Wang, Y. Li, and B. Vucetic, "Millimeter wave communications with symmetric uniform circular antenna arrays," *IEEE Commun. Lett.*, vol. 18, no. 8, pp. 1307–1310, Aug. 2014.
- [16] F. Zhang and W. Fan, "Near-field ultra-wideband mmWave channel characterization using successive cancellation beamspace UCA algorithm," *IEEE Trans. Veh. Technol.*, vol. 68, no. 8, pp. 7248–7259, Aug. 2019.
- [17] Y. Lu, C. Tao, and L. Liu, "Research on propagation characteristics of massive MIMO channel at 1.4725GHz," in *Proc. IEEE 85th Veh. Technol. Conf. (VTC Spring)*, Jun. 2017, pp. 1–5.
- [18] Y. Lu, C. Tao, L. Liu, T. Zhou, Z. Wei, and Q. Li, "Capacity of massive MIMO system based on indoor measurement," in *Proc. 12th Int. Symp. Antennas, Propag. EM Theory (ISAPE)*, Dec. 2018, pp. 1–4.
- [19] W. Chen, C. Li, J. Yu, J. Zhang, and F. Chang, "A survey of maritime communications: From the wireless channel measurements and modeling perspective," *Regional Stud. Mar. Sci.*, vol. 48, pp. 1–13, Oct. 2021.
- [20] J. Mashino, K. Tateishi, K. Muraoka, D. Kurita, S. Suyama, and Y. Kishiyama, "Maritime 5G experiment in windsurfing world cup by using 28 GHz band massive MIMO," in *Proc. IEEE 29th Annu. Int. Symp. Pers., Indoor Mobile Radio Commun. (PIMRC)*, Sep. 2018, pp. 1134–1135.
- [21] S. Wu, C. X. Wang, H. Haas, E. H. M. Aggoune, M. M. Alwakeel, and B. Ai, "A non-stationary wideband channel model for massive MIMO communication systems," *IEEE Trans. Wireless Commun.*, vol. 14, no. 3, pp. 1434–1446, Mar. 2015.
- [22] S. Wu, C.-X. Wang, E.-H.-M. Aggoune, M. M. Alwakeel, and Y. He, "A non-stationary 3-D wideband twin-cluster model for 5G massive MIMO channels," *IEEE J. Sel. Areas Commun.*, vol. 32, no. 6, pp. 1207–1218, Jun. 2014.
- [23] Y. Chen, Y. Li, S. Sun, X. Cheng, and X. Chen, "A twin-multi-ring channel model for massive MIMO system," in *Proc. 16th Int. Symp. Commun. Inf. Technol. (ISCIT)*, Sep. 2016, pp. 606–610.
- [24] J. Li, B. Ai, R. He, M. Yang, Z. Zhong, and Y. Hao, "A cluster-based channel model for massive MIMO communications in indoor hotspot scenarios," *IEEE Trans. Wireless Commun.*, vol. 18, no. 8, pp. 3856–3870, Aug. 2019.
- [25] Y. Xie, B. Li, X. Zuo, M. Yang, and Z. Yan, "A 3D geometry-based stochastic model for 5G massive MIMO channels," in *Proc. 11th EAI Int. Conf. Heterogeneous Netw. Qual., Rel., Secur. Robustness*, Aug. 2015, pp. 216–222.

- [26] J. Huang, C.-X. Wang, R. Feng, J. Sun, W. Zhang, and Y. Yang, "Multi-frequency mmWave massive MIMO channel measurements and characterization for 5G wireless communication systems," *IEEE J. Sel. Areas Commun.*, vol. 35, no. 7, pp. 1591–1605, Jul. 2017.
- [27] J. Wang, Y. Cui, S. Ma, X. Meng, and J. Teng, "A simulation model for ship-to-ship Rayleigh fading channels," in *Proc. 12th Int. Conf. Signal Process. (ICSP)*, Oct. 2014, pp. 1692–1697.
- [28] J. Wang, L. Liu, S. Ma, J. Teng, X. Meng, and Y. Cui, "A non-isotropic simulation model for ship-to-ship fading channels," in *Proc. 6th Int. Conf. Wireless, Mobile Multi-Media (ICWMMN)*, 2015, pp. 115–119.
- [29] Y. He et al., "A novel 3D non-stationary maritime wireless channel model," *IEEE Trans. Commun.*, vol. 70, no. 3, pp. 2102–2116, Mar. 2022.
- [30] A. Koc, A. Masmoudi, and T. Le-Ngoc, "Hybrid beamforming for uniform circular arrays in multi-user massive MIMO systems," in *Proc. IEEE Can. Conf. Electr. Comput. Eng. (CCECE)*, May 2019, pp. 1–4.
- [31] A. Forenza, D. J. Love, and R. W. Heath Jr., "Simplified spatial correlation models for clustered MIMO channels with different array configurations," *IEEE Trans. Veh. Technol.*, vol. 56, no. 4, pp. 1924–1934, Jul. 2007.
- [32] X. Gao, L. Dai, S. Zhou, A. M. Sayeed, and L. Hanzo, "Wideband beamspace channel estimation for millimeter-wave MIMO systems relying on lens antenna arrays," *IEEE Trans. Signal Process.*, vol. 67, no. 18, pp. 4809–4824, Sep. 2019.
- [33] A. Sayeed and J. Brady, "Beamspace MIMO channel modeling and measurement: Methodology and results at 28GHz," in *Proc. IEEE Globecom Workshops (GC Wkshps)*, Dec. 2016, pp. 1–6.
- [34] X. Xia, K. Xu, D. Zhang, Y. Xu, and Y. Wang, "Beam-domain full-duplex massive MIMO: Realizing co-time co-frequency uplink and downlink transmission in the cellular system," *IEEE Trans. Veh. Technol.*, vol. 66, no. 10, pp. 8845–8862, Oct. 2017.
- [35] F. Lai, C.-X. Wang, J. Huang, X. Gao, and F.-C. Zheng, "A novel beam domain channel model for B5G massive MIMO wireless communication systems," *IEEE Trans. Veh. Technol.*, early access, Nov. 17, 2022.
- [36] L. You, X. Gao, G. Y. Li, X.-G. Xia, and N. Ma, "BDMA for millimeter-wave/terahertz massive MIMO transmission with per-beam synchronization," *IEEE J. Sel. Areas Commun.*, vol. 35, no. 7, pp. 1550–1563, Jul. 2017.
- [37] J. Bian et al., "A novel 3D beam domain channel model for massive MIMO communication systems," *IEEE Trans. Wireless Commun.*, early access, Sep. 27, 2022, doi: 10.1109/TWC.2022.3205929.
- [38] C. Sun, X. Q. Gao, S. Jin, M. Matthaiou, Z. Ding, and C. Xiao, "Beam division multiple access transmission for massive MIMO communications," *IEEE Trans. Commun.*, vol. 63, no. 6, pp. 2170–2184, Jun. 2015.
- [39] S. Wu, C.-X. Wang, E.-H.-M. Aggoune, M. M. Alwakeel, and X. You, "A general 3-D non-stationary 5G wireless channel model," *IEEE Trans. Commun.*, vol. 66, no. 7, pp. 3065–3078, Jul. 2018.
- [40] R. Verdone and A. Zanella, *Pervasive Mobile and Ambient Wireless Communications*. London, U.K.: Springer, 2012.
- [41] J. Bian, C.-X. Wang, X. Gao, X. You, and M. Zhang, "A general 3D non-stationary wireless channel model for 5G and beyond," *IEEE Trans. Wireless Commun.*, vol. 20, no. 5, pp. 3211–3224, May 2021.
- [42] M. T. Ma, *Theory and Application of Antenna Arrays*. New York, NY, USA: Wiley, 1974.
- [43] F. Zhang, W. Fan, and G. F. Pedersen, "Frequency-invariant uniform circular array for wideband mm-Wave channel characterization," *IEEE Antennas Wireless Propag. Lett.*, vol. 16, pp. 641–644, 2017.
- [44] J. Li et al., "On 3D cluster-based channel modeling for large-scale array communications," *IEEE Trans. Wireless Commun.*, vol. 18, no. 10, pp. 4902–4914, Oct. 2019.
- [45] J. H. Brady and A. M. Sayeed, "Wideband communication with high-dimensional arrays: New results and transceiver architectures," in *Proc. IEEE Int. Conf. Commun. Workshop (ICCW)*, Jun. 2015, pp. 1042–1047.
- [46] T. Xie, L. Dai, D. W. K. Ng, and C.-B. Chae, "On the power leakage problem in millimeter-wave massive MIMO with lens antenna arrays," *IEEE Trans. Signal Process.*, vol. 67, no. 18, pp. 4730–4744, Sep. 2019.
- [47] Z. Xia, C. Qi, and T. Zhang, "Model based beamspace channel estimation for millimeter wave massive MIMO system," in *Proc. 10th Int. Conf. Wireless Commun. Signal Process. (WCSP)*, Oct. 2018, pp. 1–6.
- [48] Y. Jeon, G.-T. Gil, and Y. H. Lee, "Design and analysis of LoS-MIMO systems with uniform circular arrays," *IEEE Trans. Wireless Commun.*, vol. 20, no. 7, pp. 4527–4540, Jul. 2021.



Yubei He received the B.Sc. degree from the School of Information Science and Engineering, Shandong University, Qingdao, China, in 2017. She is currently pursuing the Ph.D. degree in information and communication engineering with Shandong University. Her current research interests include maritime communications, wireless propagation channel measurements and channel modeling, and B5G/6G wireless communications.



Cheng-Xiang Wang (Fellow, IEEE) received the B.Sc. and M.Eng. degrees in communication and information systems from Shandong University, China, in 1997 and 2000, respectively, and the Ph.D. degree in wireless communications from Aalborg University, Denmark, in 2004.

He was a Research Assistant with the Hamburg University of Technology, Hamburg, Germany, from 2000 to 2001, a Visiting Researcher with Siemens AG Mobile Phones, Munich, Germany, in 2004, and a Research Fellow with the University of Agder, Grimstad, Norway, from 2001 to 2005. He has been with Heriot-Watt University, Edinburgh, U.K., since 2005, where he was promoted to a Professor in 2011. In 2018, he joined Southeast University, Nanjing, China, as a Professor. He is currently a part-time Professor with Purple Mountain Laboratories, Nanjing. He has authored four books, three book chapters, and more than 480 papers in refereed journals and conference proceedings, including 26 highly cited papers. He has also delivered 24 invited keynote speeches/talks and 14 tutorials in international conferences. His current research interests include wireless channel measurements and modeling, 6G wireless communication networks, and electromagnetic information theory.

Dr. Wang is a member of the Academia Europaea (The Academy of Europe), a member of the European Academy of Sciences and Arts (EASA), a fellow of the Royal Society of Edinburgh (FRSE), IET, and the China Institute of Communications (CIC), an IEEE Communications Society Distinguished Lecturer in 2019 and 2020, a Highly-Cited Researcher recognized by Clarivate Analytics during 2017–2020, and one of the most cited Chinese researchers recognized by Elsevier in 2021. He is also an Executive Editorial Committee Member of the IEEE TRANSACTIONS ON WIRELESS COMMUNICATIONS. He has served as a TPC member, a TPC chair, and a general chair for more than 80 international conferences. He received 15 best paper awards from IEEE GLOBECOM 2010, IEEE ICCT 2011, ITST 2012, IEEE VTC 2013 Spring, IWCMC 2015, IWCMC 2016, IEEE/CIC ICC 2016, WPMC 2016, WOCC 2019, IWCMC 2020, WCSP 2020, CSPA2021, WCSP 2021, and IEEE/CIC ICC 2022. Also, he received the 2020–2022 "AI 2000 Most Influential Scholar Award Honorable Mention" in recognition of his outstanding and vibrant contributions in the field of Internet of Things. He has served as an Editor for over ten international journals, including the IEEE TRANSACTIONS ON WIRELESS COMMUNICATIONS from 2007 to 2009, the IEEE TRANSACTIONS ON VEHICULAR TECHNOLOGY from 2011 to 2017, and the IEEE TRANSACTIONS ON COMMUNICATIONS from 2015 to 2017. He was a Guest Editor of the IEEE JOURNAL ON SELECTED AREAS IN COMMUNICATIONS, Special Issue on Vehicular Communications and Networks (Lead Guest Editor), Special Issue on Spectrum and Energy Efficient Design of Wireless Communication Networks, and Special Issue on Airborne Communication Networks. He was also a Guest Editor of the IEEE TRANSACTIONS ON BIG DATA, Special Issue on Wireless Big Data. He is a Guest Editor of the IEEE TRANSACTIONS ON COGNITIVE COMMUNICATIONS AND NETWORKING, Special Issue on Intelligent Resource Management for 5G and Beyond.



channel modeling, and B5G/6G wireless communications.

Hengtai Chang (Member, IEEE) received the B.Sc. and Ph.D. degrees from the School of Information Science and Engineering, Shandong University, China, in 2016 and 2021, respectively. He is currently a Post-Doctoral Research Associate with Purple Mountain Laboratories, China, and also a Post-Doctoral Research Associate with the China National Mobile Communications Research Laboratory, Southeast University, China. His current research interests include UAV communications, wireless propagation channel measurements and



(ultra-) massive MIMO modeling.

Rui Feng (Member, IEEE) received the B.Sc. degree in communication engineering and the M.Eng. degree in signal and information processing from Yantai University, China, in 2011 and 2014, respectively, and the Ph.D. degree in communication and information system from Shandong University, China, in 2018. From July 2018 to September 2020, she was a Lecturer with Ludong University, China. She is currently a Post-Doctoral Research Associate with Purple Mountain Laboratories and Southeast University, China. Her research interests include

channel modeling theory and beam domain channel



at San Diego (UCSD). In 2011, he was a Visiting Scholar with Heriot-Watt University, U.K., supported by the U.K.–China Science Bridges: Research and Development on (B)4G Wireless Mobile Communications Project. His current research interests include signal processing for wireless communications, channel sounding and modeling, joint communications and sensing, maritime communication, visible light communication, and software-defined radio.

Jian Sun (Member, IEEE) received the B.Sc. degree in applied electronic technology, the M.Eng. degree in measuring and testing technologies and instruments, and the Ph.D. degree in communication and information systems from Zhejiang University, Hangzhou, China, in 1996, 1999, and 2005, respectively. From 2005 to 2018, he was a Lecturer with the School of Information Science and Engineering, Shandong University, China, where he has been an Associate Professor since 2018. In 2008, he was a

Visiting Scholar with the University of California



theory, and intelligent B5G wireless communications.

Wensheng Zhang (Member, IEEE) received the M.E. degree in electrical engineering from Shandong University, China, in 2005, and the Ph.D. degree in electrical engineering from Keio University, Japan, in 2011. He was a Visiting Scholar with the University of Oulu, Finland, in 2010, and the University of Arkansas, USA, in 2019. In 2011, he joined the School of Information Science and Engineering, Shandong University, where he is currently an Associate Professor. His research interests include tensor computing, random matrix



solutions based on novel artificial materials to reduce mutual RF interference, weight, cost, and system complexity for security, aerospace, and healthcare, with leading U.K. industries, and novel and emergent gradient index materials to reduce mass, footprint, and profile of low-frequency and broadband antennas. He also co-developed the first stable active non-Foster metamaterial to enhance usability through small antenna size, high directivity, and tunable operational frequency. He coined the term body-centric wireless communications, i.e., networking among wearable and implantable wireless sensors on the human body. He was the first to characterize and include the human body as a communication medium between on-body sensors using surface and creeping waves. He contributed to the industrial development of the first wireless sensors for healthcare monitoring. He has authored or coauthored more than 200 journal articles and has co-edited and coauthored the books *Antennas and Radio Propagation for Body-Centric Wireless Communications* (Artech House, 2006 and 2012) and *FDTD Modeling of Metamaterials: Theory and Applications* (Artech House, 2008), respectively. His research interests include computational electromagnetics, microwave metamaterials, graphene and nanomicrowaves, antennas and radio propagation for body-centric wireless networks, active antennas for millimeter/submillimeter applications, and photonic integrated antennas.

Yang Hao (Fellow, IEEE) received the Ph.D. degree in computational electromagnetics from the Centre for Communications Research, University of Bristol, Bristol, U.K., in 1998.

He was a Post-Doctoral Research Fellow with the School of Electronic, Electrical and Computer Engineering, University of Birmingham, Birmingham, U.K. He is currently a Professor of antennas and electromagnetics with the Antenna Engineering Group, Queen Mary University of London, London, U.K. He developed several fully integrated antenna

Dr. Hao is an elected fellow of the Royal Academy of Engineering, IET. He won the 2015 IET AF Harvey Research Prize and was a co-recipient of the BAE Chairman's Silver Award in 2014 and the Royal Society Wolfson Research Merit Award.



Tabuk. He coauthored papers in IEEE and other journals and conferences, and served on editorial boards and technical committees for many of them. He is listed as an inventor in several patents, one of them assigned to Boeing Company, USA. His research interests include wireless communications, sensor networks, power systems, neurocomputing, and scientific visualization. He was a recipient of the IEEE Professor of the Year Award, UW. He is a Professional Engineer registered in the state of Washington.

El-Hadi M. Aggoune (Life Senior Member, IEEE) received the M.S. and Ph.D. degrees in electrical engineering from the University of Washington (UW), Seattle, WA, USA. He worked at several universities in the USA and abroad at many academic ranks, including an Endowed Chair Professor. He was the Director of the laboratory that received the Boeing Supplier Excellence Award. He is currently working as a Professor and the Director of the Sensor Networks and Cellular Systems (SNCS) Research Center, University of